Università degli Studi di Padova

Department of Industrial Engineering

Master Thesis in Electrical Engineering

Analysis and mitigation of torque pulsations in railway traction systems

Supervisor
Silverio Bolognani
Università degli studi di Padova

Co-supervisor
Fernando Briz del Blanco
Universidad de Oviedo

Master Candidate
Anita Vegro

Academic Year: 2019/2020

ABSTRACT

High speed trains in Spain are fed by a single-phase *AC* voltage catenary line. The traction squirrel jail asynchronous motor is fed thanks to pantograph, which connects the catenary line and the single-phase step down onboard transformer. Its secondary winding feeds an active rectifier, the *DC* bus and the inverter, which output is linked with the motor. The main problem of this system is the interaction of single-phase current and single-phase voltage in the *AC-DC* converter. The interaction of these two magnitudes provokes the creation of voltage ripple at the double of grid frequency at the *DC* bus and this ripple affects the correct behaviour of the inverter and its output. Knowing that current and torque in an induction machine are linked, the problem caused from the rectifier has consequences also in the correct work of the traction motor.

Usually, an *LC* filter tuned on the second harmonic and properly dimensioned is used to limit the voltage ripple. As consequence of using the filter, it is possible to limit the *2f* torque ripple at the motor side, avoiding several bad consequences, for example the temperature increasing, power losses, torque fluctuations and pulsations, mechanical stress and vibration, audible noise. The problem of the filter is that it is heavy, bulky and expensive: it weighs on the order of few hundreds of kilos, its volume can be around some tens of litres and it costs several thousands of euros, without considering the maintenance necessity and the risk of breakage.

From this starting point, this master thesis studies a method to remove this filter and replace it with a new control for the inverter to avoid the presence of the torque ripple at the motor side.

After the first part of study and implementation of the control system considering the presence of the *2f* filter, a new algorithm has been tested in the machine model with no filter. Different working points have been tested and simulation results compared to find which method achieve the best improvement.

All simulation tests have been implemented using Matlab and Simulink.

ABSTRACT (IN ITALIANO)

Il lavoro di questa tesi magistrale prende in esame il comportamento di un sistema spagnolo di trazione elettrica ad alta velocità e, in quanto proveniente dalla penisola iberica, rispondente alle specifiche caratteristiche tecniche del luogo.

I treni ad alta velocità in Spagna vengono alimentati con grandezze alternate monofasi a 50 Hz, in analogia al sistema francese e italiano.

Il pantografo permette il collegamento tra la catenaria di alimentazione e il trasformatore monofase abbassatore a bordo treno. Al secondario di quest'ultimo sono collegati un ponte raddrizzatore, il condensatore di accumulo e quindi l'inverter per alimentare il motore asincrono a gabbia di scoiattolo, responsabile della trazione vera e propria. La presenza del raddrizzatore monofase implica all'uscita dello stesso l'insorgenza di una oscillazione alla frequenza doppia di quella fondamentale, a causa dell'interazione tra tensione e corrente, per l'appunto entrambe monofasi. Questo fenomento si ripercuote a valle del condensatore incaricato ad assorbire le fluttuazioni di tensione posto all'uscita del convertitore, lato *DC*, e compromette il corretto comportamento dell'inverter. Sia le tensioni che le correnti di fase all'uscita di quest'ultimo, infatti, risultano affette dal contenuto armonico riconducibile all'oscillazione a $2f$. Sapendo che corrente e coppia di un motore ad induzione sono strettamente correlate, l'oscillazione al doppio della frequenza di rete affligge anche il corretto comportamento del motore.

Nelle soluzioni più tradizionali, un filtro accordato a 100 Hz opportunamente dimensionato viene inserito in parallelo al condensatore lato *DC* per limitare gli effetti dannosi al motore dovuti all'oscillazione. Tra le conseguenze indesiderate per il motore che vengono evitate con l'inserimento del filtro si hanno l'aumento della temperatura, le perdite di potenza aggiuntive, pulsazioni e fluttuazioni di coppia, lo stress meccanico agli elementi circostanti, le vibrazioni meccaniche ed l'eccessivo rumore. Di contro il suddetto filtro è voluminoso e pesante, oltre ad essere costoso. Ovviamente dipende dalle caratteristiche specifiche e dalle scelte fatte in sede di progetto, ma può arrivare a pesare nell'ordine di grandezza del centinaio di chilogrammi, con un volume di qualche decina di litri e un costo di qualche migliaia di euro, senza considerare la necessità di manutenzione che richiede e il rischio di rottura.

Il lavoro legato a questa tesi nasce dal desiderio di rimuovere il filtro accordato alla seconda armonica e sostituirlo con un appropriato algoritmo di controllo per l'inverter, in modo da non avere più oscillazione di coppia al motore ed evitanto i problemi ad essa legata

sopraelencati. Inoltre rimuovendo il dispositivo di filtro ci sarebbe una notevole riduzione di peso e volume, guadagnando in posti a sedere e velocità, oltre che ad un risparmio in termini di costi.

Dopo una prima fase di studio ed approfondimento del problema e delle possibili soluzioni, sfruttando Matlab e Simulink, è stato implementato un sistema di controllo per il modello di trazione ad alta velocità preso in analisi. In un primo momento, il lavoro è stato svolto considerando la presenza del filtro *LC* nello schema, in modo da ottenere un modello affidabile e ottimizzato.

Una volta consolidato il sistema di controllo, si è potuto procedere allo studio di un algoritmo in alternativa alla presenza del filtro e all'analisi dei risultati delle simulazioni. Il sistema è stato analizzato in diverse condizioni di lavoro, quindi i risultati ottenuti sono stati paragonati a quelli ottenuti in presenza del filtro lato *DC* e confrontati tra loro per individuare in quale situazione l'algoritmo sia più o meno efficace.

ACKNOWLEDGMENTS

I'd like to thank professor Fernando Briz for his patience and his availability both during my period at the Power Electronics and Electric Drives Lab and during the quarantine period.

An hug to all guys and girls from the laboratory, there was no possibility to say goodbye by person and this is a pity.

Un sentito ringraziamento al professor Bolognani e ai suoi dottorandi per la disponibilità e la gentilezza sempre dimostrata.

Naturalmente vorrei ringraziare e abbracciare tutti coloro i quali in questi anni accademici mi abbiano supportata e anche in minima parte aiutata a superare l'ansia e ad arrivare fino a qui.

CONTENTS

LIST OF FIGURES

LIST OF TABLES

ACRONYMS

IGBT	Insulated Gate Bipolar Transistor
NPC	Neutral Point Clamped
PLL	Phase Locked Loop
PWM	Pulse Width Modulation
PR	Proportional Resonant
PI	Proportional Integrator
PID	Proportional Integrator Derivative
SOGI	Second Order Generalized Integrator
3L-NPC	Three Level Neutral Point Clamped
FOC	Field Oriented Control
IM	Induction Machine
SVM	Space Vector Modulation
SHE	Selective Harmonic Elimination
THD	Total Harmonic Distortion
EMF	Electro Magnetic Force
MTPA	Maximum Torque Per Ampere
FFT	Fast Fourier Transformation

1 INTRODUCTION

1.1 OVERVIEW

Climate change and global warming are nowadays problems that cannot be ignored anymore. Due to the continuous growth of the population and developing industrial countries, transportation demand will be one of the challenges for the future. Oil and other non-renewable energy sources are not sustainable anymore. If humanity wants to maintain the temperature increase under 1.5 °C at the end of this century as indicated by the intergovernmental panel for climate change (IPCC), technology has to adapt to change the actual trend. As reported from the Eurostat report [5], the energy consumption due transportation was almost one-third of the total global energy consumption in 2017, as reported in figure 1.1. In a green and sustainable scenario, alternative options should be competitive and preferable to traditional technologies, therefore electric and hybrid cars instead of diesel ad gasoline transportation, high speed trains instead of planes and so on.

In this kind of scenario, the use of electric trains has to be implemented and increased, therefore new studies and researches want to increase efficiency and to reduce production and maintenance costs for this *old* technology.

Electric train technology has a long story and it could be considered fully developed.

During the nineteenth century, the first electric system formed by catenary line, pantograph and electric motor appeared in the USA and in Germany. The first system fed from a catenary source was presented by Siemens and Halske during the Industrial Exposition in Berlin in 1879. It was a 3 hp motor fed by direct current at 150 V. It was the first experiment and from that moment every country tried to adapt the basic idea to the local necessity. Different ideas have been found, for example, secondary railways in Northern Italy and later on the Simplon Tunnel were electrified using three phases alternating current, solutions complicated and later eliminated (more details in [18]). Based on the nineteenth and twentieth centuries country history, different railway technologies have been developed. Today three different power systems can be found in Europe.

- 1500 or 3000 V *DC* supply, for low speed and regional trains. The main drawback for this system is the limitation of the power. It has been used since 1920s in Italy, Belgium, Poland, ...

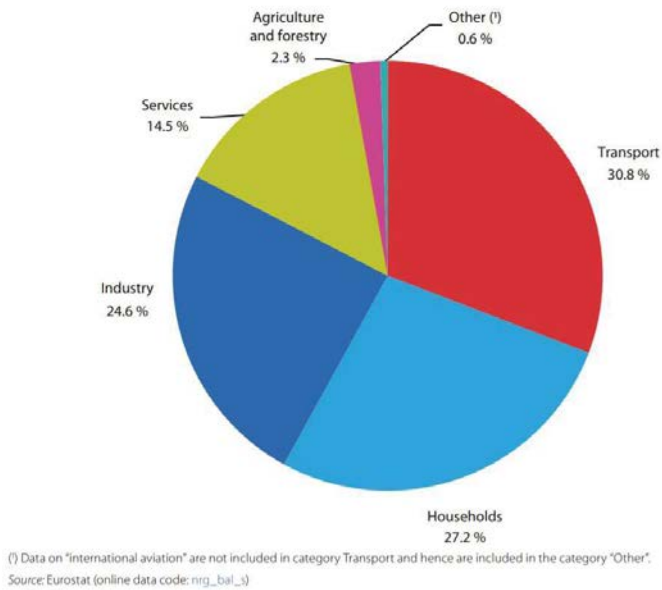

Figure 1.1: Final energy consumption by sector, EU-28, 2017.
(% of total, based on toe)

- 15 kV and 16 2/3 Hz single *AC* supply for long distance railways. Germany, Austria, Sweden, Norway and Switzerland have adopted this kind of power supply exploiting dedicated power plants to do not have frequency interferences with the national system.
- 25 kV and 50 Hz *AC* supply, for high speed trains in Spain, Italy, France and with 60 Hz frequency for example in Japan.

1.2 HIGH SPEED TRAIN

High speed trains are the main topic of this thesis. The studied model is coming from the Spanish railway system because I spent six months at the University of Oviedo.

The Spanish railway system is based on *AC* power supply, figure 1.2 represents how is composed a conventional electrical power distribution system. For this kind of configuration, a single phase step down transformer in the traction substation is used to pass from high voltage with 110 kV and 50 Hz characteristics to medium voltage, 25 kV, still frequency equal to 50 Hz. In order to have the high voltage system as balanced as possible, three consecutive transformers are connected between two different phases, for example *a-b*, *b-c*, *c-a* and then again. It is well known that an unbalanced load for a high voltage system is a problem and it can be seen as a fault and activate untimely protections.

Medium voltage lines compose the system that actually feeds the train: the system of overhead wired called catenary. The description

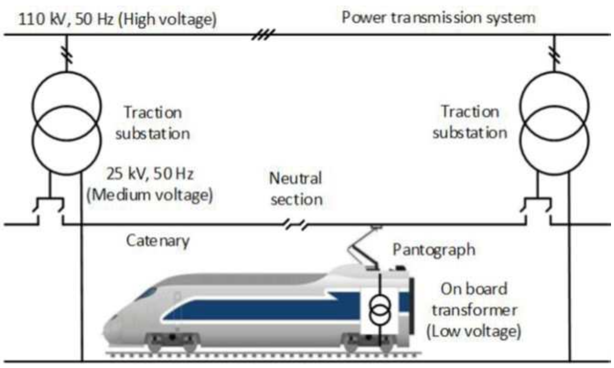

Figure 1.2: Electric power distribution system for an high speed train

of the catenary characteristics is not the purpose of this job, see [19] for more information.

The train captures the energy from the catenary line through the pantograph. The electrical connection between the catenary line and the onboard transformer is possible thanks to this device.

Explained how the system is fed, it is possible to pass to describe the onboard elements referring to figure 1.3. The figure is the general topology with which can be organized the power system of a high speed train. Although the main components remain the same as in the presented typical configuration, train manufacturers use different topologies to connect them. For example, there could be two secondary windings and rectifiers instead of one or two inverters, each designer chooses what he thinks is the best choice.

As said before, the pantograph catches the energy from the catenary line and it feeds the onboard step-down transformer. It is a 50 Hz single-phase transformer with two secondary windings and it changes the voltage value from 25 kV at the primary side to 997 V at the secondary side.

Linked with the transformer, there is a single-phase *AC-DC* controlled rectifier, used to convert the single-phase *AC* current from the catenary into *DC*. In this master thesis job, two active rectifiers are present, they are controlled through two Pulse Width Modulation (PWM) signals coming from the control system. The algorithm to maintain constant the *DC* link voltage will be deeply analyzed in the next chapters. Each active rectifier used in this model is a single-phase bridge formed by four Insulated Gate Bipolar Transistors (IGBTs) with four antiparallel diodes. These switchers have been preferred among the possibilities (GTO, Mosfet, thyristors) because their use brings some advantages. For example, IGBT is a voltage command device and not a current command one (as in the case of GTO o thyristor), for this reason the control circuit is easier in high voltage and high current applications. The electric isolation between command and power is guaranteed and it sustains maximum voltages of $2 \div 3$ kV range and currents of $2 \div 3$ kA, the voltage drop is limited to $2 \div 3$

V, [12]. Although IGBTs have small switching time, they can sustain lower commutation frequency then Mosfets, but this is not a big issue for this kind of application.

The *DC* voltage has to be transformed again into *AC* because the traction motor needs to be fed by a three phase voltage to work properly. This operation is made using a three level three phase inverter controlled using a sinusoidal PWM technique with homopolar injection, the controlled system will be analyzed later on this master job. The inverter is composed of three legs, each leg is composed of four IGBTs with four antiparallel diodes and two more diodes to have the access to the middle voltage point, in fact this kind of converter is called Neutral Point Clamped (NPC) inverter. Connected to the output of the inverter there is the traction machine, it is a squirrel jail induction motor. It can work in four quadrants and so braking energy could be recovered and be stored at the *DC* bus in the capacitor through the inverter, which can work in all quadrants too.

It is well known that two different voltage sources cannot be disposed in a parallel topology if their values are not coincident each time step, otherwise the system would collapse. For this reason, the *AC-DC* rectifier and the *DC-AC* inverter cannot be directly connected and a capacitor between them is necessary. This capacitor absorbs harmonic contents and stabilizes the *DC* link voltage. It has to be big enough to guarantee that the voltage ripple satisfies the requirements of the rule but not that big to be too much heavy or expensive, a trade-off analysis is necessary.

The last element that usually is present in the traction system of a high speed train is the *LC* filter. It is a filter tuned to reduce the second harmonic component which is present because the *AC-DC* rectifier is a single-phase converter and the interaction of voltage and current causes this problem, as it will be described in chapter 2. This filter is bulky, heavy, voluminous and expensive, therefore train companies started to study a way to remove it, looking for a control strategy to obtain a motor behaviour without harmonic content at the double of catenary frequency even if this element is not present.

Table 1.1 presents the most important characteristics of the system analyzed in this master's thesis.

1.3 MASTER THESIS GOAL

This master project studies the possibility to remove the *2f* filter from a train and replace it by electric drives control strategy for the inverter. This thesis job takes two previous works [21] and [16] as a starting point and as reference for the more detailed characteristics of the system, for example, resistance and inductance data for the induction machine.

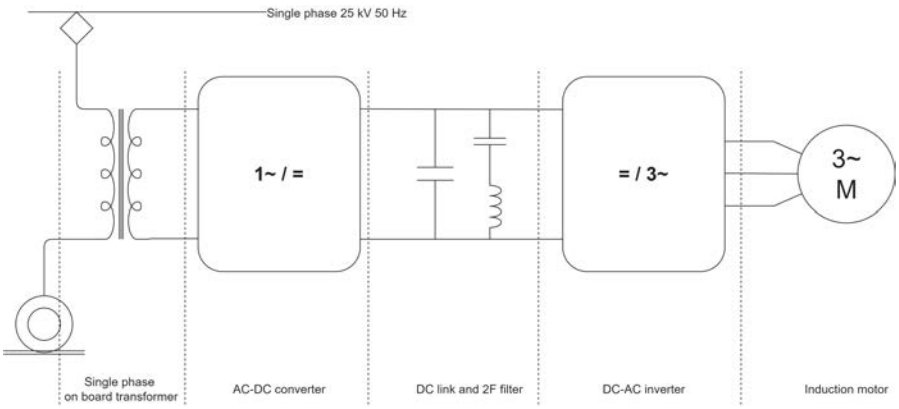

Figure 1.3: Schematic on board train representation

Table 1.1: Main characteristics of the system

Part	Size	Value
Transformer	V_{pri}	25000 [V]
	V_{sec}	997 [V]
	f_{grid}	50 [Hz]
DC bus	V_{DC}	1800 [V]
	C_{DC}	0.011 [F]
Induction motor	S_{nom}	220.6 [kW]
	V_{s_rated}	1270 [V]
	pf	0.8066
	p	2
	η_{rated}	0.96

The first part of the job has been related to the implementation of the control strategy with the presence of the *2f* filter to have a solid and well working system. After this part, the system has been studied without the filter, trying to implement some controls from the bibliography and evaluating results in different conditions.

The structure of the thesis can be divided into steps corresponding to the work phases.

1. understanding the ripple problem for this kind of system and how it affects the behaviour of the motor;

2. implementation of the closed-loop control of the system considering the presence of the *2f* filter in the model;

3. analysis of possible methods to replace the filter with control system;

4. removing the filter and studying of the behaviour with new controls through different simulation conditions.

2 THE RIPPLE PROBLEM

The goal of the project is to study a simulation model and an efficient control system for high speed AC drives for electric traction, in order to minimize the harmonic contents and power ripple at the motor side. The most important target of this job is to find a method to replace the *2f* filter at the *DC* bus with a control algorithm for the inverter to remove the power ripple detectable in the motor. The first step is understanding why this ripple is present and where it comes from.

The system is fed from a single-phase voltage, this brings an input power which fluctuates at twice the catenary frequency. The mathematical reason is now explained.

2.1 DC LINK

The instantaneous supply voltage and current can be expressed with equations (2.1) and (2.2) respectively.
Figure 2.1 shows the simplified diagram of the system: it represents the catenary source $v_s(t)$, the *AC-DC* rectifier and the *DC* bus, the inverter and induction motor are included in the load. The presence of the *LC* filter will be discussed later.

$$v_s(t) = \sqrt{2}V_{rms}\sin(\omega t) \tag{2.1}$$

$$i_s(t) = \sqrt{2}I_{rms}\sin(\omega t + \varphi) \tag{2.2}$$

where $\omega = 2\pi f$, f is the catenary frequency $f = 50\,\text{Hz}$, V_m and I_m voltage and current peak values and φ is the angle between voltage and current.
The converter input power is obtained multiplying the voltage and the current, the result (2.3) shows a continuous component P_{const} and

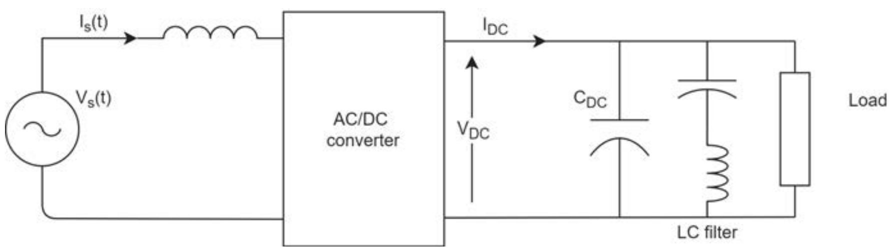

Figure 2.1: Diagram representation of the system.

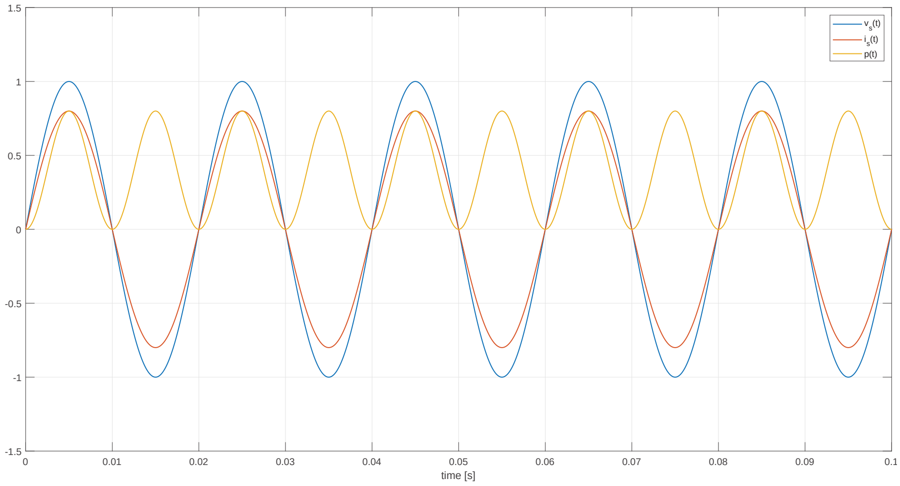

(a) *Voltage, current and power with no phase angle shift hypothesis*

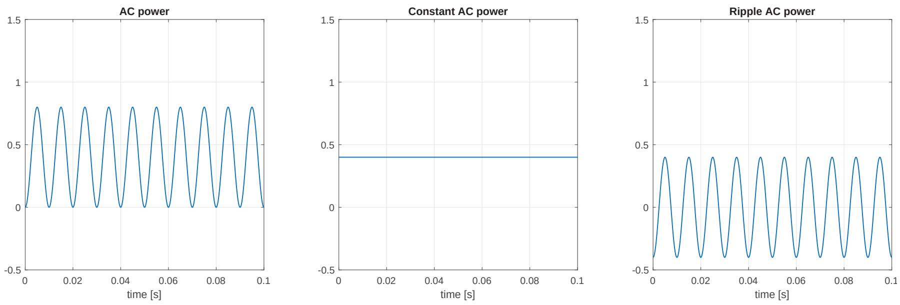

(b) *Total power: its constant part and its the ripple part*

Figure 2.2: Voltage, current and power (above). Power focus (below)

an oscillating component p_{ripple}. This AC component is presenting the frequency twice the catenary frequency.
A graphic representation of voltage, current and power is presented in fig. 2.2, it is assumed that voltage and current don't have phase shift, i.e. $\varphi = 0$.

$$\begin{aligned} p_{AC}(t) &= v_s(t)\, i_s(t) = \\ &= V_{rms}\, I_{rms} \cos\varphi - V_{rms}\, I_{rms} \cos(2\omega t + \varphi) = \\ &= P_{const} + p_{ripple} \end{aligned} \tag{2.3}$$

Assuming that there are no power losses from the input and the output of the *AC-DC* converter, $p_{AC}(t)$ is equal to P_{DC} and this means that the *2f* ripple is transferred to the DC bus. The way to express the instantaneous *DC* power is generally represented as it is shown in (2.4), the constant part of the power is transferred to feed the active components of the load, while the pulsating component pulses and it feeds the *DC* smoothing capacitor C_{DC}. This ripple of power has to be filtered using a resonant *LC* supply.

$$P_{DC} = p_{AC}(t) = V_{DC}\, I_{DC} + V_{DC}\, C_{DC} \frac{d\, v_C}{dt} \tag{2.4}$$

The constant component P_{const} from the *AC* side is equal to the constant component at the *DC* side, so (2.5) can be deduced. Similarly, equation (2.6) can be found.

$$I_{DC}\, V_{DC} = V_{rms}\, I_{rms} \cos\varphi$$

$$\frac{I_{DC}}{\cos\varphi} = \frac{V\, I}{V_{DC}} \tag{2.5}$$

$$V_{DC} C_{DC} \frac{d\, v_C}{dt} = V\, I \cos(2\omega t + \varphi) \tag{2.6}$$

By substituting and going on with mathematical steps, equation (2.8) can be obtained.

$$\frac{d\, v_C}{dt} = \frac{I_{DC}}{\cos\varphi} [\frac{\cos(2\omega t + \varphi)}{C_{DC}}] \tag{2.7}$$

$$\begin{aligned} v_C(t) &= \int \frac{I_{DC}}{\cos\varphi} \left[\frac{\cos(2\omega t + \varphi)}{C_{DC}}\right] dt = \\ &= \left(\frac{I_{DC}}{2\omega\, C_{DC}\, \cos\varphi}\right) \sin(2\omega t + \varphi) = \\ &= (\Delta V_{DC}) \sin(2\omega t + \varphi) \end{aligned} \tag{2.8}$$

In the end, the instantaneous *DC* link voltage can be express as the sum of the two components, the constant one and the oscillating one (eq. (2.9)). It is clear the amplitude value of the ripple from (2.8), see (2.10).

$$v_{DC}(t) = V_{DC} + v_C(t) = V_{DC} + \left(\Delta V_{DC}\right) \sin(2\omega t + \varphi) \tag{2.9}$$

$$\Delta V_{DC} = \frac{I_{DC}}{2\omega\, C_{DC}\, \cos\varphi} \tag{2.10}$$

This voltage ripple has to be small and it has to respect normative rules, otherwise this oscillation will have consequences in all the downstream power system. In order to reduce this beat phenomenon different technical devices are taken:

- increasing the number of rectifiers with the same transformer, the higher is the number of converters the lower is the beat effect;
- choosing an appropriate *DC* capacitor, it absorbs voltage fluctuation between two voltage sources;
- adding an *LF* filter tuned for the second harmonic. The behaviour of the system with and without the filter is one of the object of this thesis work.

2.2 BEAT EFFECT

The ripple affects the *DC* bus, it is absorbed by capacitor but this oscillation has consequences also downstream, causing problems to the inverter output and the correct work of the induction motor. The reasons are now presented referring to articles [6] and [7].
The inverter output voltages are calculated as the product of the source voltage (2.9) and the switching function of the inverter $S_{inv}(t)$.

$$S_{inv}(t) = \frac{1}{2} + \sum_{k=odd}^{\infty} A_{vk} \cos k(\omega_s t + \phi_v) \qquad \text{where } v = a, b, c \quad (2.11)$$

$$A_{vk} = \frac{2(-1)^{\frac{k-1}{2}}}{k\pi}$$

Considering eq. (2.11), ω_s is the fundamental angular frequency of the output voltage of inverter and $\phi_v = \{0; 2\pi/3; 4\pi/3\}$ and the coefficient A_{vk} is inverse proportional to kw_s.
The inverter output phase voltages referring to the hypothetical neutral point of the power source $v_{vo}(t)$ can be calculated as follow, see (2.12).

$$\begin{aligned} v_{vo}(t) = v_{DC}(t)\,(S_{inv} - 1/2) = V_{DC} \sum_{k=odd}^{\infty} A_{vk} \cos k(\omega_s t + \phi_v) + \\ + \frac{\Delta V_{DC}}{2} \sum_{k=odd}^{\infty} A_{vk} \Big\{ \sin\Big[(2\omega_g + k\omega_s)t + \phi + k\phi_v\Big] + \\ + \sin\Big[(2\omega_g - k\omega_s)t + \phi - k\phi_v\Big] \Big\} \end{aligned} \quad (2.12)$$

In this last equation, the first part shows the fundamental component and the harmonic components which are produced by the average *DC* link voltage, while the second term represents the harmonic

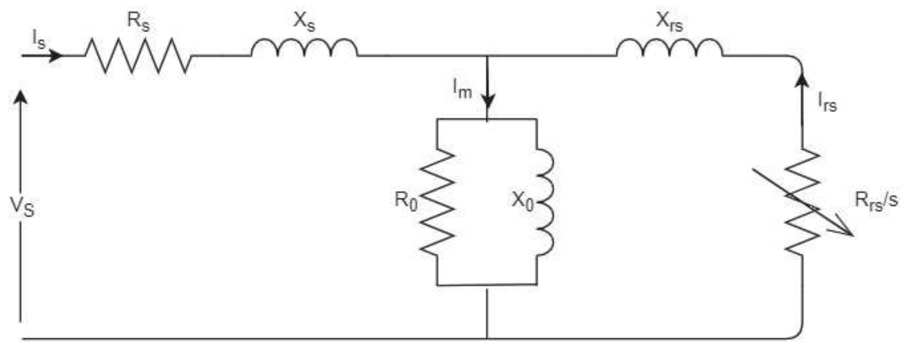

Figure 2.3: Induction motor equivalent scheme

components caused by the voltage oscillation seen in the previous section. The beat component due the *DC* voltage ripple is transferred to the inverter output and it corresponds to the angular frequency $2\omega_{grid} \pm k\omega_s$.

High frequency components are small because A_{vk} is inversely proportional to the frequency, on the other hand, the lower frequency voltage is not neglectable. This affects the impedance of the induction motor.

The equivalent circuit of the traction motor in fig. 2.3 is taken as reference model and the impedance is now evaluated.
If the resistance and the motor inductance are constant with the frequency, the impedance from the primary side is presented as a function of angular frequency and slip.

$$\dot{Z}_m = \dot{Z}_m(\omega, s) \tag{2.13}$$

When the motor rotating speed is considering constant and it is $\omega = (1 - s_i)\omega_i$, with s_i fundamental slip, the k-th harmonic impedance is expressed by (2.14). Similarly the beat component impedance (2.15) is found.

$$\dot{Z}_{mk} = \dot{Z}_m\left(\omega = n\omega_i,\ s = 1 - \frac{1 - s_i}{k}\right) \tag{2.14}$$

$$\dot{Z}_{mk\pm} = \dot{Z}_m\left(\omega = 2\omega_{grid} \pm n\omega_i,\ s = 1 - \frac{(1 - s_i)\omega_i}{2\omega_{grid} \pm n\omega_i}\right) \tag{2.15}$$

Considering (2.12), (2.14) and (2.15), the phase current can be found.

$$
\begin{aligned}
i_{vo}(t) = \frac{V_{DC}}{Z_{mk}} \sum_{k=odd}^{\infty} A_{vk} \cos k(\omega_s t + \phi_v - \phi_{zk}) + \\
+ \Delta V_{DC} \sum_{k=odd}^{\infty} A_{vk} \left\{ \frac{1}{Z_{mk+}} \sin\left[(2\omega_g + k\omega_s)t + \phi + k\phi_v - \phi_{zk+}\right] + \right. \\
\left. + \frac{1}{Z_{mk-}} \sin\left[(2\omega_g - k\omega_s)t + \phi - k\phi_v - \phi_{zk-}\right] \right\}
\end{aligned}
\tag{2.16}
$$

where $Z_{mk(\pm)} = \left|\dot{Z}_{mk(\pm)}\right|$ and $\phi_{zk(\pm)} = \angle \dot{Z}_{mk(\pm)}$.

The second term on the left-hand side (eq. (2.16)) represents the beat phenomenon component. Torque and phase currents are strictly correlated, therefore they have the same kind of harmonics. When the inverter output frequency of the inverter is close to the *DC* ripple frequency, i.e. when $(2\omega_{grid} - k\omega_s)$ tend to zero, the motor impedance is very small and beat problems occur.

Many harmful events are linked with this beat phenomenon, such as temperature increase, additional power losses, torque pulsation and fluctuation, mechanical stress on connected components, severe mechanical vibrations and acoustic noise. All these phenomena have to be avoided, generally it is used a filter *LC*, but there are some ideas to implement a beatless control system and to do not use this heavy and costly filter, as we will see later.

2.3 2F FILTER

As it is said in section 2.1, it is necessary a technique to limit the ripple on the *DC* bus. Generally, it is used filter tuned on the second harmonic (i.e. at $f_c = 100$ Hz), this device is composed by a capacitor C_f and an inductance L_f. These two elements are chosen to satisfy the eq. (2.17) and after a trade-off study on cost, weight and volume.

$$
f_c = \frac{1}{2\pi\sqrt{L_f C_f}} \tag{2.17}
$$

As the target of engineering is to obtain the better results the lower amount of resources, research and development are also related with saving costs, being this the reason why companies spend money in improving its current technologies. Rightly, removing the *2f* filter involves savings in cost as well as in weight and volume. Usually, inductance and capacitance for railway applications are in the range of millihenry [mH] and millifarad [mF], therefore they are bulky and voluminous and they take a lot of space on trains. Together they can weight around some hundreds of kilos and their volume can be around 30-40 litres, so finding a way to avoid to install this device on the train is good option to take the best advantage from the catenary energy because the locomotive carriage is lighter. At last, this filter can cost some thousands of euros and there is the breaking possibility like any other power electronic device, it needs its cooling system and maintenance plan. For all these reasons a beatless control is necessary to improve the high speed technology and to bring the performances to the edge.

3 CONTROL SYSTEM

In this chapter the control system will be deeply analysed, figure 3.1 is the starting point, each section will now be explained.

Each part of this and result chapters have been studied and implemented using Matlab and Simulink.

3.1 ACTIVE RECTIFIER

The first part of control strategy is focused on the control of the Active Rectifier, which is the power supply needed to pass from catenary single-phase *AC* voltage to *DC* magnitudes. It is an active system because it has to ensure that the output will follow the given reference with the minimum steady state error.

Figure 3.2 shows the converter electric scheme. The active rectifier is a full bridge converter composed by four switchers IGBT, the catenary source is simplified using an *AC* voltage source with its impedance, the inverter and the induction motor are represented by the *RC* parallel load.

The block diagram to control the rectifier is illustrated in fig. 3.3. The control system is based on a current loop which has both as input and output an *AC* signal. The current loop is controlled in turn by a voltage loop, this last one works with constant signals. In order to have a synchronous sinusoidal signal, a Phase Locked Loop (PLL) is necessary, as we will see later. The diagram output is the reference for the PWM generator to control the full bridge. Remember that switchers T_1 and T_2 are working together, T_3 and T_4 together with opposite behaviour.

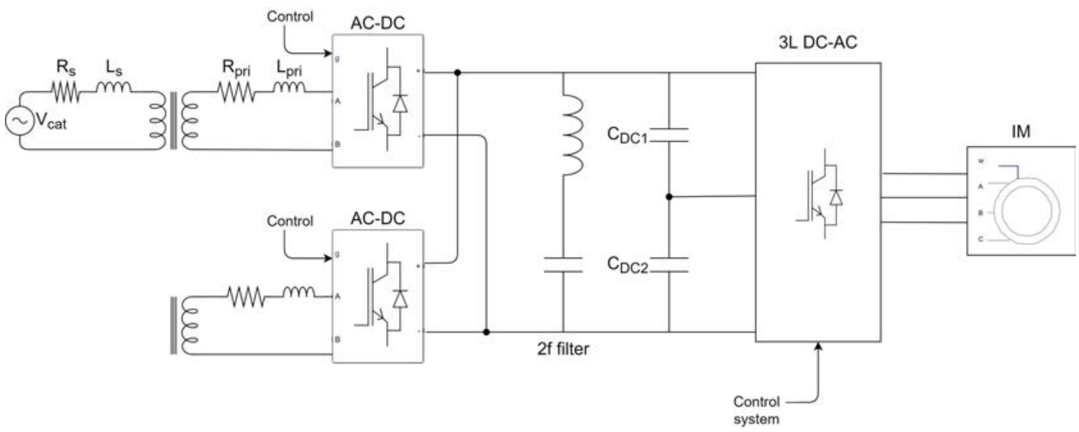

Figure 3.1: Complete electric scheme

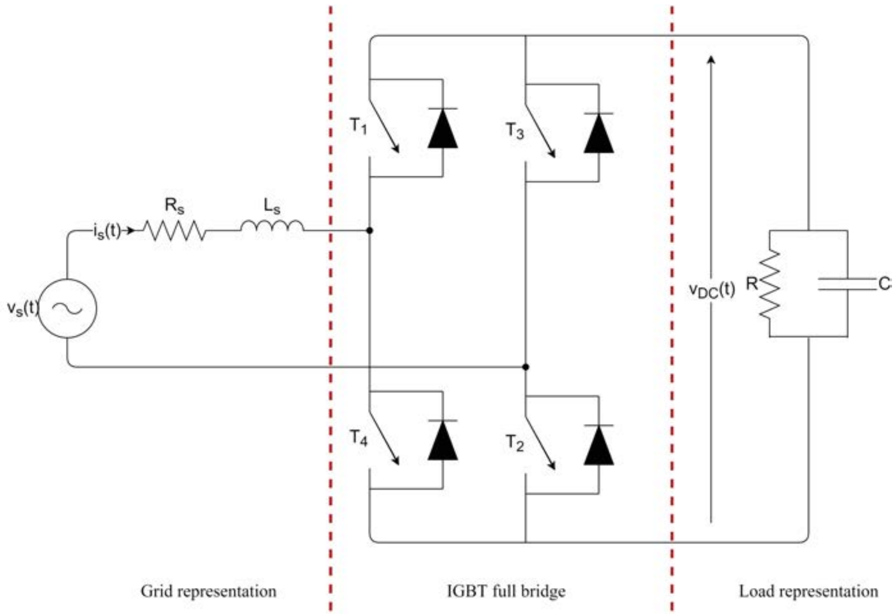

Figure 3.2: Rectifier system

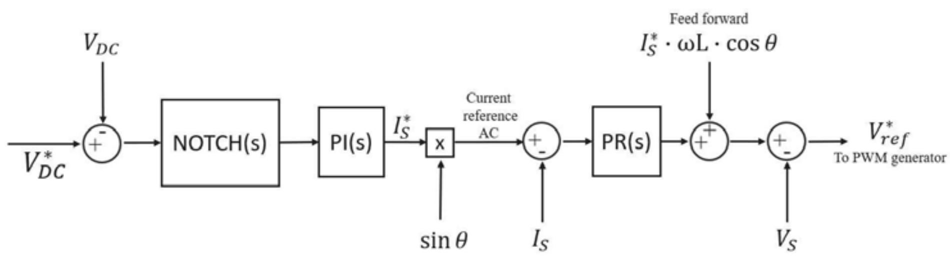

Figure 3.3: Control block diagram

For the current controller, a Proportional Resonant (PR) controller is necessary because the input signal is not constant. The infinite gain is required at 50 Hz frequency, not at 0 Hz frequency. Using this kind of controller unit power factor can be obtained avoiding *dq* from *abc* reference system transformation. The transfer function of the resonant controller is reported in eq. (3.1), zero-pole cancellation is the method used to tune it (more details in [3]).

$$PR(s) = 2k_p \frac{s^2 + \frac{s}{\tau_i} + \omega_l^2}{s^2 + \omega_l^2} \tag{3.1}$$

where $k_p = 2\pi \cdot bw \cdot L_s$ is the gain; $bw = 500\,Hz$ the bandwidth [rad/s] and $\omega_l = 2\pi \cdot f$ the resonance frequency. Note that $f = 50$ Hz. $\tau_i = L_s/R_s$ is the time constant.

In a single-phase system like the one studied, there is less information than in a three-phase system regarding the grid condition, but the necessity that the current follows the voltage still there. A Phase Locked Loop (PLL) can provide a unitary power factor operation to synchronize the output current with the grid voltage and to give a clean sinusoidal reference. The general structure of a single-phase PLL is extrapolated from [2]. The same paper presents a method to generate an orthogonal voltage system through a Second Order Generalized Integrator (SOGI), from this signal couple it is quite easy to pass from $\alpha\beta$ to dq reference. The q component is fixed to zero using a Proportional Integrator (PI) controller, the phase angle is obtained integrating this value added to frequency reference. The controller is designed to achieve a fast response and to have high bandwidth. Fig. 3.5 explains how it works showing input and output examples.

Zero-pole cancellation using a simple PI controller is used for voltage loop, it is designed assuming an RC parallel load as representation of the downstream system.

$$PI(s) = k_{Pv} + k_{Iv} \cdot \frac{1}{s} \tag{3.2}$$

Where $k_{Pv} = 2\pi \cdot bw \cdot C$ as proportional gain and $k_{Iv} = 2\pi \cdot bw/R$ as integral gain. $bw = 10$ Hz voltage bandwidth, C, R are the load parameters.

The presence of $2f$ ripple on the DC bus is a problem as said before, for this reason a *notch* filter is added. This is a band block filter that passes most frequencies unaltered, but attenuates those in a specific range to very low levels, in this specific case $f_{del} = 2f = 100$ Hz.

$$H(s) = \frac{s^2 + \omega_0^2}{s^2 + \omega_C s + \omega_0^2} \tag{3.3}$$

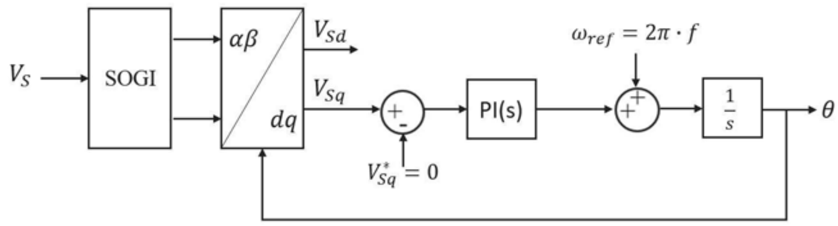

Figure 3.4: Phase lock loop block diagram

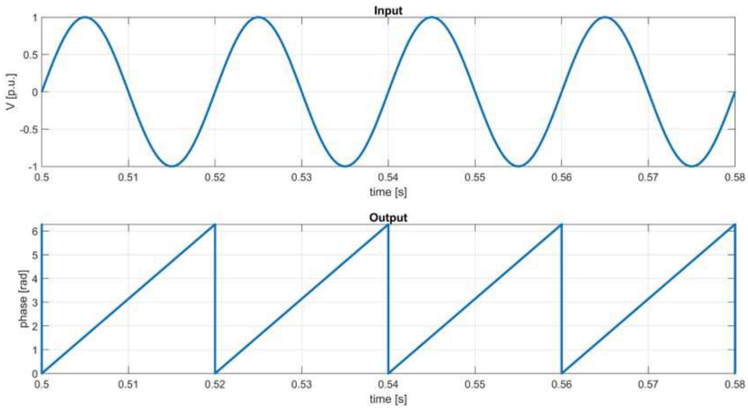

Figure 3.5: PLL input and output

Where $\omega_0 = 2\pi \cdot f_{del}$ is the central rejected frequency and $\omega_C = 2\pi \cdot bw$ is the cut off frequency. The bandwidth is $bw = 20\,Hz$.

3.2 DC BUS

The target voltage for the *DC* bus is 1800 V. The *AC-DC* converter is not ideal and its output is not constant, it oscillates around high frequencies and it has a relevant second harmonic component, as it is explained in chapter 2.

It is not possible to create a parallel link between two subsystems that have different instantaneous voltage, for this reason, a capacitor component is necessary, it absorbs the voltage fluctuation from both the *AC-DC* converter and *DC-AC* inverter.

As said before, the higher number of converters, the lower second harmonic ripple is introduced by rectifiers and the higher number of secondary windings for the transformer. It should be a trade-off.

In this first part of the study and control implementation, the *2f* filter is used in order to be sure that the control system is reliable.

The presence of a three-level inverter requires an access to the middle point voltage and for this reason two capacitors are used

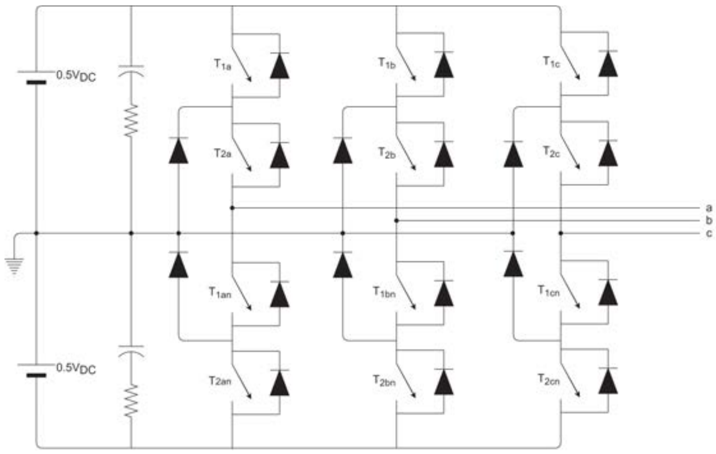

Figure 3.6: Three level inverter

instead of a single one. These two are in a serial disposition, they have the same value $C_{DC1} = C_{DC2} = 2C_{DC}$, where C_{DC} is the entire capacity value to filter the harmonics content. This conclusion is the direct consequence of eq. (3.4).

$$\begin{aligned} \frac{1}{\omega\, C_{eq}} &= \frac{1}{\omega\, C_{DC1}} + \frac{1}{\omega\, C_{DC2}} \\ C_{eq} &= \frac{C_{DC1}\, C_{DC2}}{C_{DC1} + C_{DC2}} = C_{DC} \end{aligned} \tag{3.4}$$

3.3 THREE LEVEL INVERTER

Figure 3.6 shows the inverter used in the project. It is a Three Level Neutral Point Clamped (3L-NPC), its output can assume three different values respect the ground reference or a central voltage reference. Each leg is formed by four IGBTs with antiparallel diodes and two diodes to have the access to the middle voltage.

The three-level inverter is a way to achieve a higher converter efficiency and to have better technical performances than the two-level. Classic two-level inverters have problems when the voltages are high, when lots of commutations per period are required because the harmonic content gets worse and when dV/dt is high (parasitic effects). In order to overcome these problems and to fulfil control performance requirements, three-level inverter has been preferred for this project.

The benefits of using three-level converter are not only limited to the converter itself. The three-level output voltage waveform is smoother because it can change amongst three different values, this fact helps to limit the upstream electromagnetic interference phenomenon linked with current harmonics. Also on the machine side, the harmonic losses are reduced considerably and so there is less additional heating and

Table 3.1: Switchers command and correspondent voltage

V_{aO}	T_1	T_2	$\bar{T}_1$	$\bar{T}_2$
$\mathbf{V_{DC}/2}$	1	1	0	0
$\mathbf{0}$	0	1	1	0
$\mathbf{-V_{DC}/2}$	0	0	1	0

less machine isolation stress. Three-level inverter use reduces the motor acoustic noise and ideally it is necessary no machine de-rating.

On the other side, the control of a three-level inverter is more complicate, the use of space vector modulation is difficult and it is used a multi-level PWM technique, different phase dispositions are available. More elements are necessary than a two-level inverter, $2 \times (N-1)$ switchers per leg and $(N-1) \times (N-2)$ diodes, considering that each one has the same reverse nominal voltage $V_{DC}/(N-1)$. $N = 3$, level number. Another drawback in three-level adoption is that there are not appreciable benefits for low power working point, this argument is studied in detail in [17] and [11].

Table 3.1 shows how switchers work, T_1 and T_2 are the upper one and $\bar{T}_1$, $\bar{T}_2$ the lowest ones. The signal reference is modulated through two triangular carriers, one from 0 to 1, while the other one from -1 to 0, simply vertically shifted (see fig. 3.7). The output is used to control the inverter switchers ([20]).

Homopolar harmonic injection technique is used to avoid as long as it is possible the entering in over-modulation region commanding the inverter. Considering that a homopolar signal does not change the space vector (moreover this one has null average value) it is possible to command the inverter between $-V_{DC}/2$ and $V_{DC}/2$ injecting $v_h(t)$, a triangular waveform with three times frequency. In this way, the PWM modulation still works properly, but the peak value of the first harmonic increases from $V_{DC}/2$ to $V_{DC}/\sqrt{3}$, like what it can be obtained with space vector modulation. The homopolar component ($\hat{v}_h = V_{DC}/4\sqrt{3}$) balances the distances between the voltage command and the PWM triangular carrier and the average voltage does not change before and after the injection. Fig. 3.8 and fig. 3.9 show how the sine wave is transformed and the block diagram to obtain it on Simulink.

The general PWM command has $V_{DC}/2$ as maximum, while it is possible to obtain $V_{DC}/\sqrt{3}$ with space vector modulation.

Appendix A reports a comparison between the use of two-level inverter with different modulation techniques and three-level inverter with sinusoidal pulse width modulation technique with homopolar injection. Both inverters are included in the same control model.

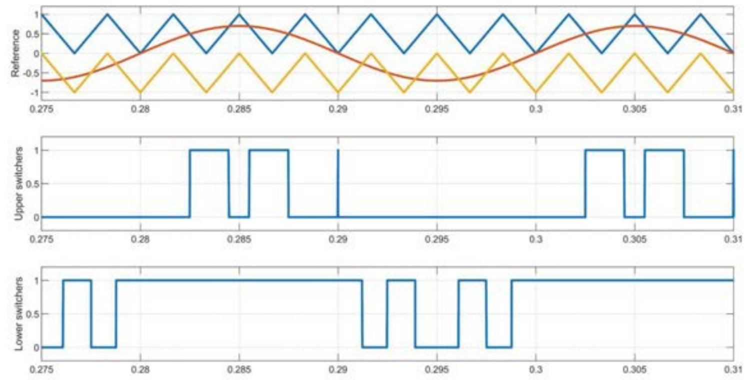

Figure 3.7: Level-shifted PWM

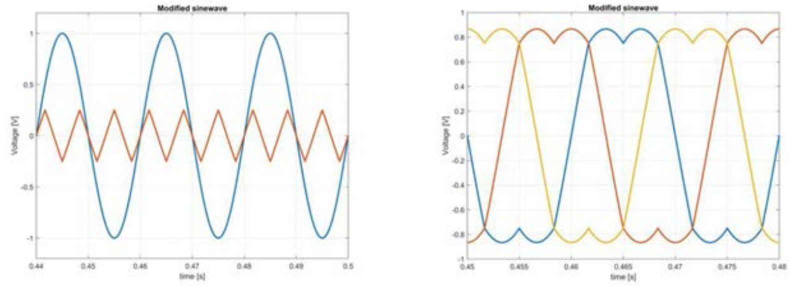

(a) *Sinewave and homopolar injection*

(b) *Modified sinewave*

Figure 3.8: Before and after triple harmonic injection

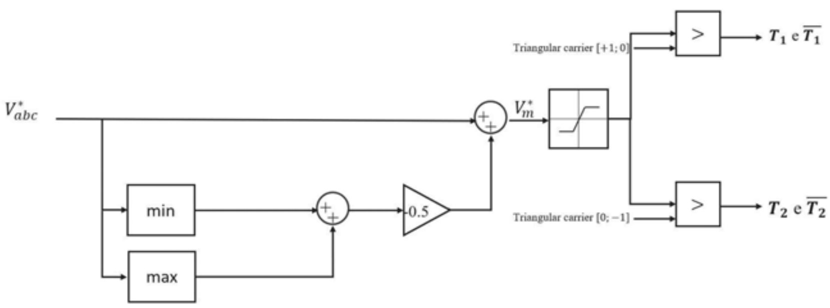

Figure 3.9: Homopolar harmonic injection block diagram

3.4 MACHINE CURRENT CONTROL

The general torque and the flux dynamics equations for an induction machine are respectively (3.5) and (3.6).

$$T = \frac{3}{2} p \frac{L_m}{L_r} (i_{sq}\lambda_{rd} - i_{sd}\lambda_{rq}) \tag{3.5}$$

$$\frac{1}{2}\frac{d\lambda_r^2}{dt} + \frac{R_r}{L_r}\lambda_r^2 = \frac{R_r L_m}{L_r}(i_{sd}\lambda_{rd} + i_{sq}\lambda_{rq}) \tag{3.6}$$

where p is the pairs pole number, L_m and L_r machine parameters, λ_{rd} and λ_{rq} are d and q components of the rotor flux λ_r in a generic reference frame and i_{sd} and i_{sq} are stator current components.

It is clear that there is mutual interference between real and imaginary component, problems occurs when you want to study the system and built a current control system.

Considering that there are infinite solutions to select the angle of the synchronous reference frame (all of the reference frames rotate at the same speed in steady state conditions), it is chosen a reference which has the d-axis aligned with the rotor flux. In this way, d-axis controls the flux component and q-axis controls the torque. This technique is called Field Oriented Control (FOC) (for more information [1]).

Flux and torque can be controlled separately by i_{sd} and i_{sq}, this is possible only if $\lambda_{rq} = 0$. Equations (3.5) and (3.6) become (3.7) and (3.8).

$$T = \frac{3}{2} p \frac{L_m}{L_r} i_{sq}\lambda_{rd} \tag{3.7}$$

$$\frac{1}{2}\frac{d\lambda_r^2}{dt} + \frac{R_r}{L_r}\lambda_r^2 = \frac{R_r L_m}{L_r} i_{sd}\lambda_{rd} \tag{3.8}$$

The main problem of FOC implementation is the necessity of knowing the rotor flux complex vector, but the rotor is usually not accessible. The rotor flux vector must be estimated from machine equations and measurable data.

Indirect and direct are the two possible algorithms to have the angle θ_s that fixes the reference frame and the rotor flux. The indirect algorithm uses the machine model and it imposes conditions to have d-axis coincident with λ_r. The direct algorithm estimates the rotor flux from easy measurements from the machine.

In this model, a direct algorithm to estimate the rotor flux is used exploiting stator current and rotor speed values. This method can operate at any speed, including zero speed, stator currents are not a

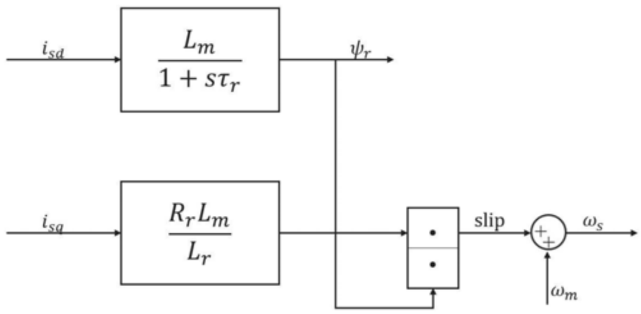

Figure 3.10: Flux extimator

problem, the main problem is the rotor speed knowledge. Furthermore, rotor resistance changes with temperature and rotor inductance is affected by iron saturation.

Figure 3.10 represents the estimator block diagram, as said before it has stator current and rotor speed as input and rotor flux and reference angle as output.

Once found rotor flux and reference frame angle, a cascaded control loop is tuned in order to obtain voltage references needed to manage the inverter's IGBTs. Figure 3.11 shows the block diagram used to control the torque of the squirrel jail asynchronous machine installed on the studied system. The inner part is a current controlled loop and the outer one is a flux loop for the d-axis and a torque loop for the q-axis.

The flux reference is compared with the estimated one from the FOC algorithm, the error is the input for the flux PI controller. The output is the reference to be compared with the d component of the measured current (obtained after an *abc* to *dqo* reference frame transformation) and the error goes to the current PI controller.

On the other hand, the q-axis has to control the torque component. Considering that in FOC conditions $T = \frac{3}{2}p\frac{L_m}{L_r}i_{sq}\lambda_{rd}$, the q-axis reference for the stator current can be obtained dividing the torque demand by $\frac{3}{2}p\frac{L_m}{L_r}\lambda_{rd} = \frac{3}{2}p\frac{L_m}{L_r}\lambda_r$. This value is compared with the measured one (also in this case after *abc* to *dqo* transformation) and the current error is the input for another PI controller.

Current controllers are tuned through zero pole cancellation considering (3.9) as transfer function for the q-axis and (3.10) for the d-axis.

$$Y_q(s) = \frac{1}{R_s} \cdot \frac{1}{1+\sigma\tau_s s} \tag{3.9}$$

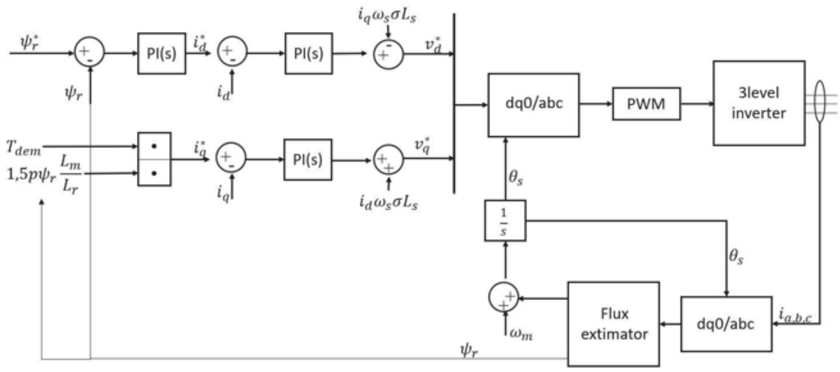

Figure 3.11: IM current control block diagram

$$Y_d(s) = \frac{1}{R_s} \cdot \frac{1 + \tau_r s}{1 + (\tau_r + \tau_s)s + \sigma\tau_r\tau_s s^2} \tag{3.10}$$

where $\sigma = L_t/L_s$, $L_t = L_s - L_m^2/L_r$ is the transient stator synchronous inductance, $\tau_r = L_r/R_r$ rotor time constant, $\tau_s = L_s/R_s$ stator time constant, R_s, L_s, R_r, L_r and L_m are stator, rotor and mutual parameters.

Axis decoupling factor is added downstream of the PI controllers and before *dqo* to *abc* reference transformation in order to have a better performance.

Finally, the voltage reference can be transformed into *abc* coordinates and used to control the inverter through sinusoidal Pulse Width Modulation (PWM) technique.

4 BEATLESS CONTROL STRATEGIES

After having an appropriate and accurate control system with *2f* filter, two methods have been studied to replace it with an improved control system for the inverter. Chapter 2 is considered as a starting point to analyse this possibility.

4.1 SWITCHING FUNCTION TO SUPPRESS THE BEAT PHENOMENON

The beat phenomenon of motor current is caused mainly by the low-frequency side-band voltage produced by the ripple component of the power source voltage. The elimination of the low frequency $(\omega_0 - \omega_s)$-component from the inverter output voltage is possible controlling the switching frequency. Remember that $\omega_0 = 2\omega_{grid}$.

The switching function can be divided into fundamental component S_{v0} and additional component thought to eliminate the side-band component ΔS_v.

$$S_{inv} = 1/2 + S_{v0} + \Delta S_v \qquad \text{where } v = a, b, c \tag{4.1}$$

Substituting eq. (4.1) into eq. (2.12) at page 10, the inverter output results:

$$v_{vo}(t) = v_{DC}(S_{v0} + \Delta S_v) \tag{4.2}$$

If

$$S_{v0} = A\cos(\omega_s t + \phi_v) \tag{4.3}$$

the inverter output voltage from eq. (4.2) becomes (4.4).

$$\begin{aligned} v_{vo} =& AV_{DC}\cos(\omega_s t + \phi_v) + \frac{A\Delta V_{DC}}{2}\Big\{\cos\big[(\omega_0 + \omega_s)t + \phi_0 + \phi_v\big] + \\ &+ \cos\big[(\omega_0 - \omega_s)t + \phi_0 - \phi_v\big] + \\ &+ V_{DC}\Delta S_v + \Delta V_{DC}\Delta S_v\cos(\omega_0 t + \phi_0)\Big\} \end{aligned} \tag{4.4}$$

where A represents a constant which varies with pulse mode, $A = 2/\pi$ for single pulse mode.

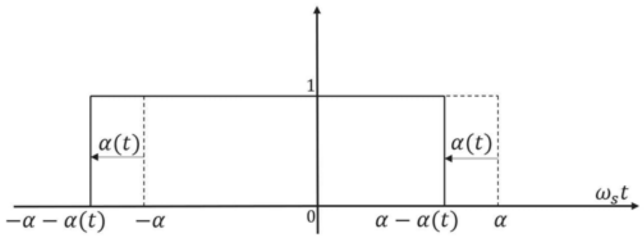

Figure 4.1: Frequency modulation switching function

The elimination of the $(\omega_0 - \omega_s)$-component from the inverter output voltage is possible letting

$$\Delta S_v = -\frac{A\delta}{4}\cos[(\omega_0 - \omega_s)t + \phi_0 - \phi_v] \tag{4.5}$$

where $\delta = 2\Delta V_{DC}/V_{DC}$.
Naturally, the line voltage contains no $(\omega_0 - \omega_s)$-component if it is eliminated from the terminal voltage.

4.2 BEATLESS CONTROL BASED ON THE FREQUENCY MODULATION SCHEME

The switching function (4.5) can be realized with frequency modulation. With this technique, the inverter frequency is varied following a specific time function. In this way, the commutation phase angles at rise time and fall time vary according to time function $\alpha(t)$ to generate the specific harmonic component of the switching function. Using other words, the inverter frequency is superimposed a compensation component according to time function $\alpha(t)$.
This scheme in principle is the same as the pulse phase modulation used for selective harmonic elimination methods to cancel specific components. In this scheme the inverter is modulated at the ripple frequency of power source, moreover the circuit is very simple.

Defining $\omega_s t = \theta$, the switching function reported in fig. 4.1 is expanded into a Fourier series.

$$S(\theta) = \frac{1}{2} + \sum_{k=odd}^{\infty} A_k \cos k\theta \tag{4.6}$$

$$A_{vk} = \frac{2(-1)^{\frac{k-1}{2}}}{k\pi}$$

If

$$\theta(t) = \omega_s t + \alpha(t) \tag{4.7}$$

then the switching function (4.6) becomes the following (4.8).

$$S(t) = \frac{1}{2} + \sum_{k=odd}^{\infty} A_k \cos k[\omega_s t + \alpha(t)] \tag{4.8}$$

In addition, if

$$\alpha(t) = \frac{2\pi \Delta F_c}{\omega_c} \sin(\omega_c t + \phi_c) \tag{4.9}$$

then the instantaneous inverter frequency f_i can be writter as eq. (4.10).

$$\begin{aligned} f_i &= \frac{1}{2\pi}\omega(t) = \frac{1}{2\pi}\frac{d}{dt}\theta(t) = \\ &= F_s + \Delta F_c \cos(\omega_c t + \phi_c) \end{aligned} \tag{4.10}$$

where ΔF_c is the frequency modulation index and F_s is the average inverter frequency. ω_c is the modulating angular frequency and ϕ_c is the modulating phase angle.

Equations 4.8 and 4.9 give the following equation, $C_c = 2\pi \Delta F_c / \omega_c$.

$$\begin{aligned} S(t) = \frac{1}{2} + \sum_{k=odd}^{\infty} A_k \Big\{ & \cos k\omega_s t \cos\{kC_c[\sin(\omega_c t + \phi_c)]\} + \\ & - \sin k\omega_s t \sin\{kC_c[\sin(\omega_c t + \phi_c)]\} \Big\} \end{aligned} \tag{4.11}$$

As reported in [13] and [7], the equation (4.11) can be written as equation (4.12) considering $J_n(x)$, the n order Bessel function.

$$\begin{aligned} S(t) = \frac{1}{2} + \sum_{k=odd}^{\infty} A_k \Big\{ & J_0(kC_c) \cos k\omega_s t + \\ & + \sum_{n=1}^{\infty} J_n(kC_c)\{\cos[(n\omega_c + k\omega_s)t + n\phi_c] + \\ & + (-1)^n \cos[(n\omega_c - k\omega_s)t + n\phi_c] \Big\} \end{aligned} \tag{4.12}$$

The frequency component $(\omega_c - \omega_s)$ component should be eliminated, this is possible setting ω_c at ω_0. Considering $k = 1$, Bessel approximations $J_0(C) = 1$ and $J_1(C) = 1/2$ and neglecting $J_n(x)(n \geq 2)$, equation (4.12) becomes (4.13).

$$\begin{aligned} S(t) = \frac{1}{2} + A_1 \Big\{ &\cos \omega_s t + \\ &+ \frac{C_c}{2} \{\cos[(\omega_c + \omega_s)t + \phi_c] - \cos[(\omega_c - \omega_s)t + \phi_c]\} \Big\} \end{aligned} \tag{4.13}$$

Once again, if the modulating angular frequency ω_c is set at ω_0, it is possible to obtain the component required for beat elimination.

The output phase voltage of inverter is deduced as

$$\begin{aligned} v_{ao} = v_{DC}(S_{inv} - 1/2) = &V_{DC} A_{a1} \cos \omega_s t + \\ &+ \frac{\Delta V_{DC} A_{a1} + V_{DC} A_{a1} C_c}{2} \cos[(\omega_c + \omega_s)t + \phi_c] + \\ &+ \frac{\Delta V_{DC} A_{a1} - V_{DC} A_{a1} C_c}{2} \cos[(\omega_c - \omega_s)t + \phi_c] + \\ &\frac{\Delta V_{DC} A_{a1} C_c}{4} \cos[(2\omega_c + \omega_s)t + 2\phi_c] + \\ &- \frac{\Delta V_{DC} A_{a1} C_c}{4} \cos[(2\omega_c - \omega_s)t + 2\phi_c] \end{aligned} \tag{4.14}$$

In order to eliminate the $(\omega_c - \omega_s)$-component, the multiplicative coefficient before the sinusoidal function must be zero.

$$\frac{\Delta V_{DC} A_{a1} - V_{DC} A_{a1} C_c}{2} = 0 \tag{4.15}$$

and so $\Delta V_{DC} = V_{DC} C_c$.

Substituting $C_c = 2\pi \Delta F_c / \omega_c$, then

$$\Delta F_c = \frac{\omega_r}{2\pi} \frac{\Delta V_{DC}}{V_{DC}} \tag{4.16}$$

As it is clear from equation (4.14) and it is also explained in [9], in the output phase voltage of inverter the harmonic ripple that creates problems $\omega_c - \omega_s = 2\omega_{grid} - \omega_s$ can be eliminated, but $2\omega_c \pm \omega_s = 4\omega_{grid} \pm \omega_s$ harmonic ripples are introduced. Their amplitudes are greatly attenuated, but these components cannot be eliminated.

Proposed solutions

Amongst the proposed solutions, I found three implementable schemes to remove the beat component using the frequency modulation technique and therefore in the scheme model which do not consider the *2f* filter.

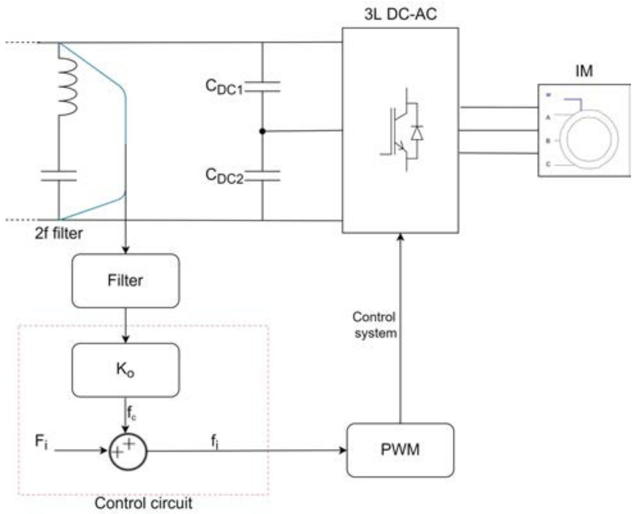

Figure 4.2: First frequency modulation block diagram

1. The first is proposed by [13], the ripple of the power source voltage is detected through a filter and the control circuit produces the inverter frequency compensation f_c (second term on the right-hand side of eq. (4.10)). This term is added to average inverter frequency F_i to produce the instantaneous f_i. Figure 4.2 represents this scheme.

2. The second solution is proposed in [7]. As figure 4.3 shows, it is based on a bandpass filter and a compensation factor, *BPF* and K_r.

3. The third solution is presented in [9] and it is reported in fig. 4.4. A PLL system detects the fluctuating *DC* voltage and this one is used to calculate the compensation frequency. Moreover, on this beatless frequency compensation method, a PR controller is used to suppress the new ripple voltage, i.e the one from $2\omega_c \pm \omega_s = 4\omega_{grid} \pm \omega_s$.

4.3 BEATLESS CONTROL BASED ON THE FEEDBACK MODULATION SCHEME

This kind of control removes the beat phenomenon moving the modulation wave that commands the inverter. Feedback compensation's target is to use the ripple of instantaneous stator current feedback to suppress beat phenomenon, using real-time monitoring of the motor current and command current as feedback to correct the modulation index.

As demonstrated in the previous sections, the beat phenomenon is transmitted downstream and it affects the motor too. For this reason, it is logical to say that control loops are affected by the beat effect.

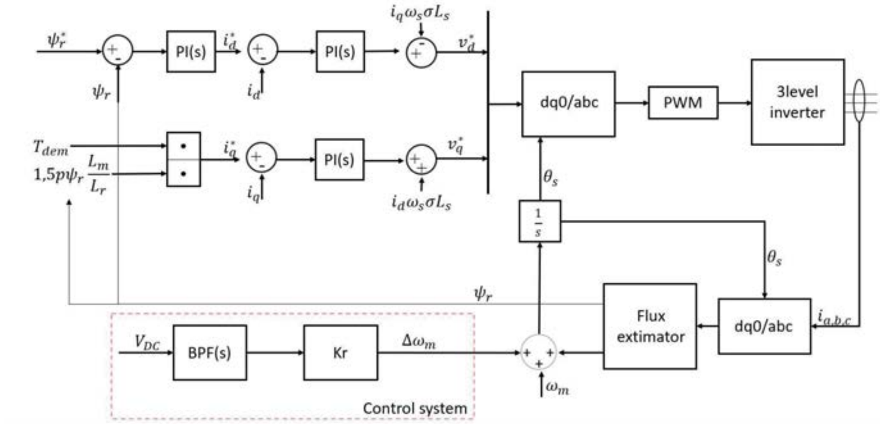

Figure 4.3: Second frequency modulation block diagram

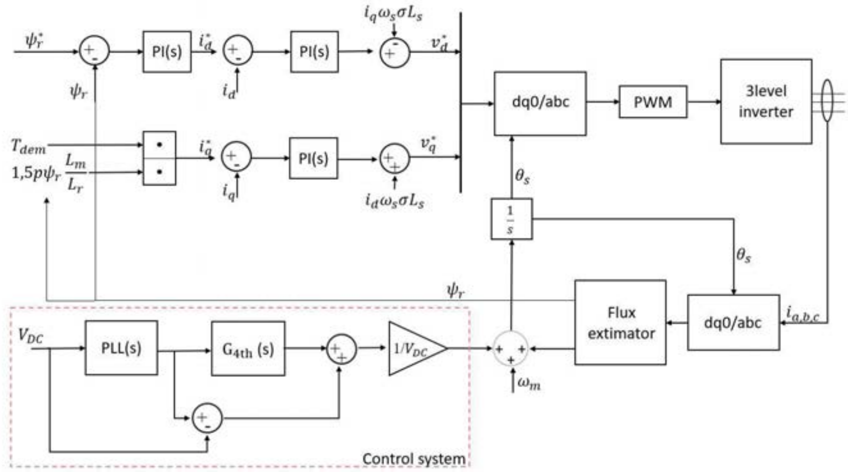

Figure 4.4: Third frequency modulation block diagram

Assuming that the q-axis current contains two fluctuating components, it can be expressed as follows.

$$i_q^* = I_q \sin(\omega_l t) \sin(2\omega_{grid} t) \tag{4.17}$$

where I_q is the amplitude of q-axis current, ω_l is the angular frequency of the load torque ripple and ω_{grid} the grid angular frequency.

According to the relationship between the stationary reference frame and the rotor dq-reference frame, the motor current can be expressed as

$$i_v = \sqrt{\frac{2}{3}}[i_d \cos\phi - i_q \sin\phi] \tag{4.18}$$

The angle ϕ can be expressed as $\phi = \omega_i t + \theta_0$, with θ_0 initial electrical angle of the motor. Substituting from (4.17) and ϕ to (4.18), it can be written:

$$\begin{aligned} i_v &= i_{u1} + i_{u2} = \\ &= \sqrt{\frac{2}{3}} i_d \cos(\omega_i t + \theta_0) + \\ &- \sqrt{\frac{2}{3}} I_q \sin(\omega_l t) \sin(2\omega_{grid} t) \sin(\omega_i t + \theta_0) \end{aligned} \tag{4.19}$$

It is clear that the d-axis current does not contain ripple components, only the q-axis component composing the motor current is taken into account when the motor beat current is taken into consideration. The second term can be simplified using the product to sum formula (mathematical passages from [22])

$$\begin{aligned} i_{u2} &= \sqrt{\frac{2}{3}} I_q \sin(\omega_l t) \sin(2\omega_{grid} t) \sin(\omega_i t + \theta_0) \\ &= \frac{I_q}{2\sqrt{6}} \sin[(\omega_l + 2\omega_{grid} + \omega_i)t + \theta_0] + \\ &- \frac{I_q}{2\sqrt{6}} \sin[(\omega_l + 2\omega_{grid} - \omega_i)t - \theta_0] + \\ &- \frac{I_q}{2\sqrt{6}} \sin[(\omega_l - 2\omega_{grid} + \omega_i)t + \theta_0] + \\ &+ \frac{I_q}{2\sqrt{6}} \sin[(\omega_l - 2\omega_{grid} - \omega_i)t - \theta_0] \end{aligned} \tag{4.20}$$

The second term on the right-hand side in (4.20) is exactly the beat component causing unnecessary losses and influencing system performances. It is possible to eliminate harmonics at $2f$ from stator current and torque pulsation compensating the q-axis current.

Proposed solutions

Amongst the proposed solutions, I found four implementable schemes to remove the beat component using feedback implementation in a scheme where the $2f$ filter is not presented.

1. The paper [14] presents a method which changes the modulation index in the inverter control modulation. If the output currents are sinusoidal and balanced, the amplitude of the vector $\mathbf{I_0}$, $|\mathbf{I_0}| = \sqrt{\frac{2}{3}[i_a^2 + i_b^2 + i_c^2]}$ will be constant. On the other hand, if the output current will be distorted by low order harmonics from the *DC* link, this magnitude will not be constant. For the implementation scheme, the magnitude of $\mathbf{I_0}$ is compared with the magnitude of the reference current, the error feeds a PI controller, its output is the modulation index for the space vector modulation (see figure 4.5).
   A disadvantage of this technique is the controller tuning, it has to be precise, otherwise the control will be not good enough.

2. The same idea of the previous method is implemented in [4], in this case, a PWM control is used and the method suitably changes the switching frequency in order to achieve the immunity to the *DC* link voltage ripple. This new function modifies the instantaneous values of the inverter modulating signal and through this the inverter input current harmonics are computed with the correction technique. In this way the inverter output voltage does not present lower order harmonics.

3. A third proposal is presented in [23]: a closed-loop sinusoidal PWM control method with real-time waveform feedback technique. The voltage disturbances are not measured and only the output current is sampled through a low pass filter. Current is compared with the reference and the error feeds a PI or a Proportional Integrator Derivative (PID) controller tuned to reject disturbances. The PID controller is introduced to have an extra grade of freedom and reduce both overshoot and rise time. Block diagram presented in figure 4.6.

4. The last method is presented in [22] and maybe it is the easiest one to implement. It is based on the theory seen at the beginning of this section. This beat-less controller is realized by moving the modulation wave up and down, this modifies the turn-on and the turn-off time of the inverter's IGBTs. In particular, the turn-on time of upper IGBTs increases and the turn-on time of lower IGBTs

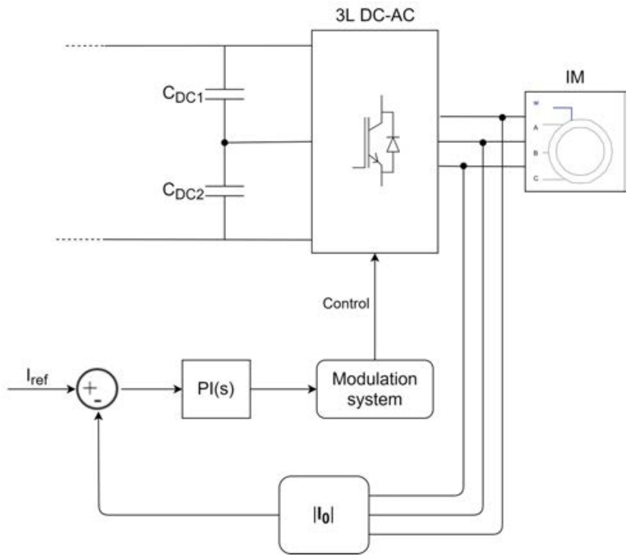

Figure 4.5: First feedback block diagram

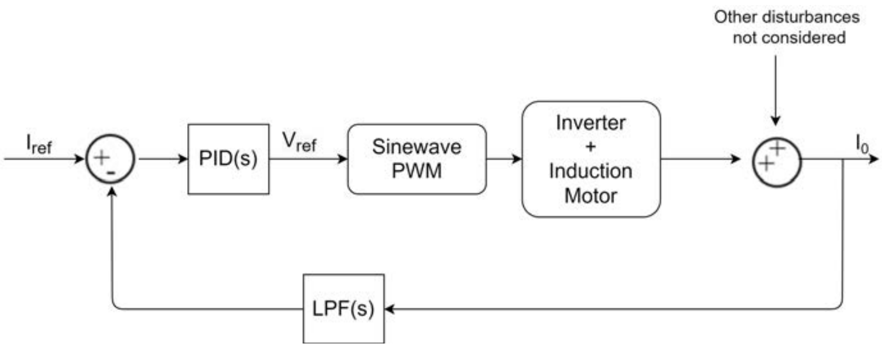

Figure 4.6: Third feedback block diagram

decreases when moving the modulation wave up, the contrary when it moves down. The deviation in motor voltage caused by the *DC* bus voltage ripple can be eliminated by the deviation caused by moving the modulation wave. In this way, the ripples of the motor torque and the motor current are both eliminated. The block diagram is reported in figure 4.7.

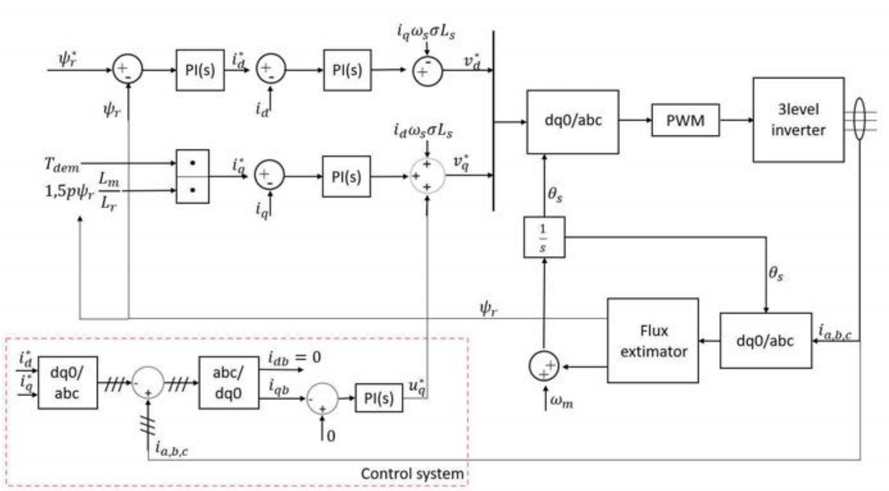

Figure 4.7: Forth feedback block diagram

5 SIMULATION RESULTS

When a machine and its control has to be tested, it has to be spliced with a load machine, like it is represented in fig. 5.1.
The Induction Machine (IM) is the test machine, it can be controlled through torque (T) or speed (ω), similarly the load machine fixes torque or speed. There are four combinations to command the system. If both the control and the load machine impose torque or speed, the system cannot work in the case of the reference value and load value are different. Using torque specifications the test machine will accelerate all the time, while using speed specifications the control action will reach its limits trying to achieve the target speed and this is not possible because the load machine will not allow it.
There are two feasible choices. The first considers that the load machine sets the load torque and the control is made through a speed control loop. The second choice is the one implemented in this master job: the load machine fixes the speed and the control uses the torque demand. In this strategy, slip and electrical frequency will be proportional to the torque.

According to papers, in order to see better the $2f$ ripple in the output of the inverter and the motor, the machine should have the rotor speed near 100 Hz. The nominal speed for this IM is just under 50 Hz, therefore it is necessary to use a field weakening technique.

Below the rated speed, it is possible to work in the constant torque region using rated flux (unless you want to implement Maximum Torque Per Ampere (MTPA) algorithm, for more information see [8]) and the applied voltage grows linearly proportional to the speed due to the back Electro Magnetic Force (EMF). When the machine reaches nominal speed, the voltage available in the output of the converter reaches its limit.

Considering eq. (5.1), the only way to increment the rotor speed having fixed maximum back EMF is reducing the rotor flux. In FOC conditions, flux has a directly proportional relation with i_d d-axis

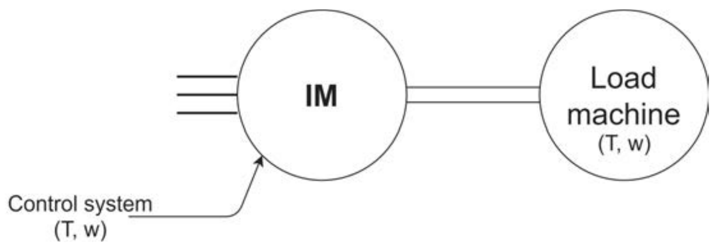

Figure 5.1: Test system

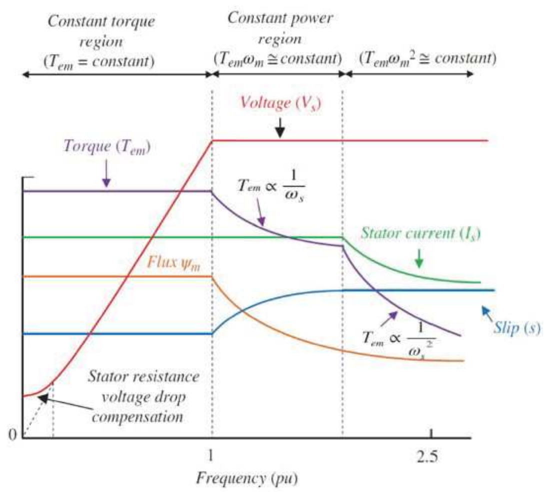

Figure 5.2: Motor magnitudes represent in the speed range of the motor [1]

current, therefore field weakening is managed by d-axis. When the machine reaches the nominal speed, the rotor flux is reduced by a reduction in the d-axis current, and that way the back EMF problem is also reduced allowing the controller to get more speed from the machine, with the same voltage applied.

$$Bemf = \frac{L_m}{L_r}\omega_r\lambda_r \tag{5.1}$$

Figure 5.2 shows different IM operating areas and how field weakening works. As said before, the induction motor works with constant torque condition until the rotor speed (and so the frequency) reaches the nominal value. Stator current, flux and slip are constant too, voltage is the only value which increments linearly. Above the nominal rotor speed, the voltage cannot grow anymore and the IM works with constant power conditions: torque and flux decrease inversely proportional to the speed. In the last region, also stator currents decrease with very high speed.

In this work, the actual flux follows the following equation.

$$\lambda_{actual}(\omega_r) = \lambda_{rated}\frac{\omega_{rated}}{\omega_r} \tag{5.2}$$

Remember that operating above the rated speed, the output of the q-axis regulator can saturate if the flux is too high. On the contrary, if the flux is too low, the q-axis output will be far from the limit and so the controller will not work properly.

5.1 CLOSED LOOP CONTROL SYSTEM

In this first part of the result description, some graphs are reported to prove that the control system theoretically described in chapter 3 is working properly.

The system is considered with:

- without the *2f* filter at *DC* bus side;
- load speed $\omega_r = 70$ Hz;
- torque demand $T_{dem} = 0,9 \cdot T_{rated}$.

The effects of the control for the *AC-DC* rectifiers are verifiable considering their output and how it follows the reference. Figure 5.3 shows the *DC* bus voltage and how it evolves during the time simulation. The big oscillation around $2,5$ seconds is due to the start of the speed from the load machine. The oscillation is limited even when the motor is reaching the target values. In the next section the ripple problem will be discussed in more detail.

The control to regulate the inverter behaviour is presented in detail in section 3.4. Figure 5.4 shows how the system follows the references and therefore how much PI controllers are accurate. The first graph represents the rotor flux reference and how the actual one follows it, the second row shows the references for the currents and the behaviour of the actual i_d and i_q. The third graph shows the output of d-axis and q-axis voltages in the same image, these values are then changed through *dq0-abc* reference system transformation and they are the reference magnitudes for the sinusoidal PWM.

Figure 5.5 shows the behaviour of output inverter currents and phase to neutral voltages. The harmonic content of currents is low and this is not a big issue considering that the equivalent impedance of the motor is resistant inductive type. It is evident from the voltage representation that the inverter is a three-level one because each wave assumes three different values $\{-1800; 0; 1800\}$.

In the end, figure 5.6 represents how the IM meets the requirements, the torque follows the reference even considering speed higher than the nominal one.

Looking more deeply into figure 5.5, it seems that currents and voltages present low-frequency components in addition to others. These low-frequency components do not derive from the *DC* bus, their presence could be explained referring to [15] and [10]. Figure 5.7 presents the FFT analysis of stator voltage and current, emphasising these components.

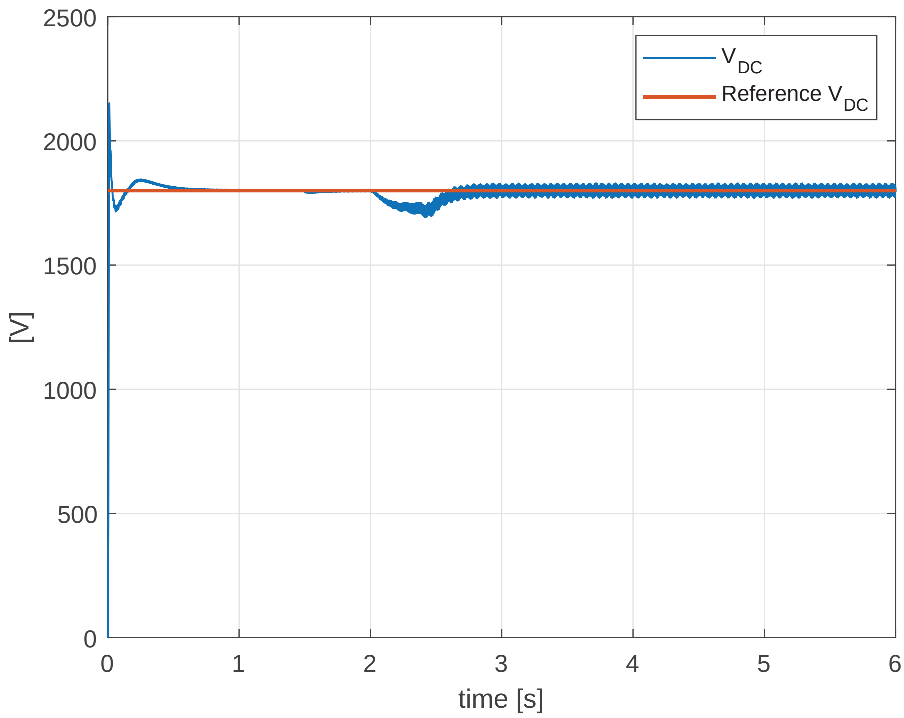

Figure 5.3: Reference and actual DC voltage

5.2 SYSTEM ANALYSIS WITH AND WITHOUT 2F FILTER

The *LC* filter presence affects to remove the *2f* component in the *DC* bus voltage and in the motor torque, as largely said in chapter 2. In this section these two magnitudes are reported and analysed considering the presence or not of the *2f* filter in the system. All the other conditions (torque demand, machine load speed) are fixed.

In order to have a better comprehension of the harmonic content, the signals have been studied using the Fast Fourier Transformation (FFT) analysis. In general, Fourier transformation takes a signal and breaks is down into sine waves of different amplitudes and frequencies. The FFT analysis is an optimized implementation of a discrete Fourier transformation, which produces as result the frequency domain components of the input signal. The fast Fourier (FFT) takes less computation to perform compared to discrete Fourier transformation, but essentially they get the same result.

Figure 5.8 and 5.9 report the *DC* bus voltage with and without *2f* filter respectively. In these figures, the first row represents the voltage trend as a time function, the second and the third row represent the FFT analysis in the normal reference system and the logarithmic one. In these last two graphs, the constant component is not reported because its value is much bigger compared to the other harmonic magnitudes.

Figures 5.10 and 5.11 shows the difference of *2f* harmonic magnitude on the voltage. It is evident the presence of the ripple when the filter is removed. This behaviour is obvious, the filter was designed to remove

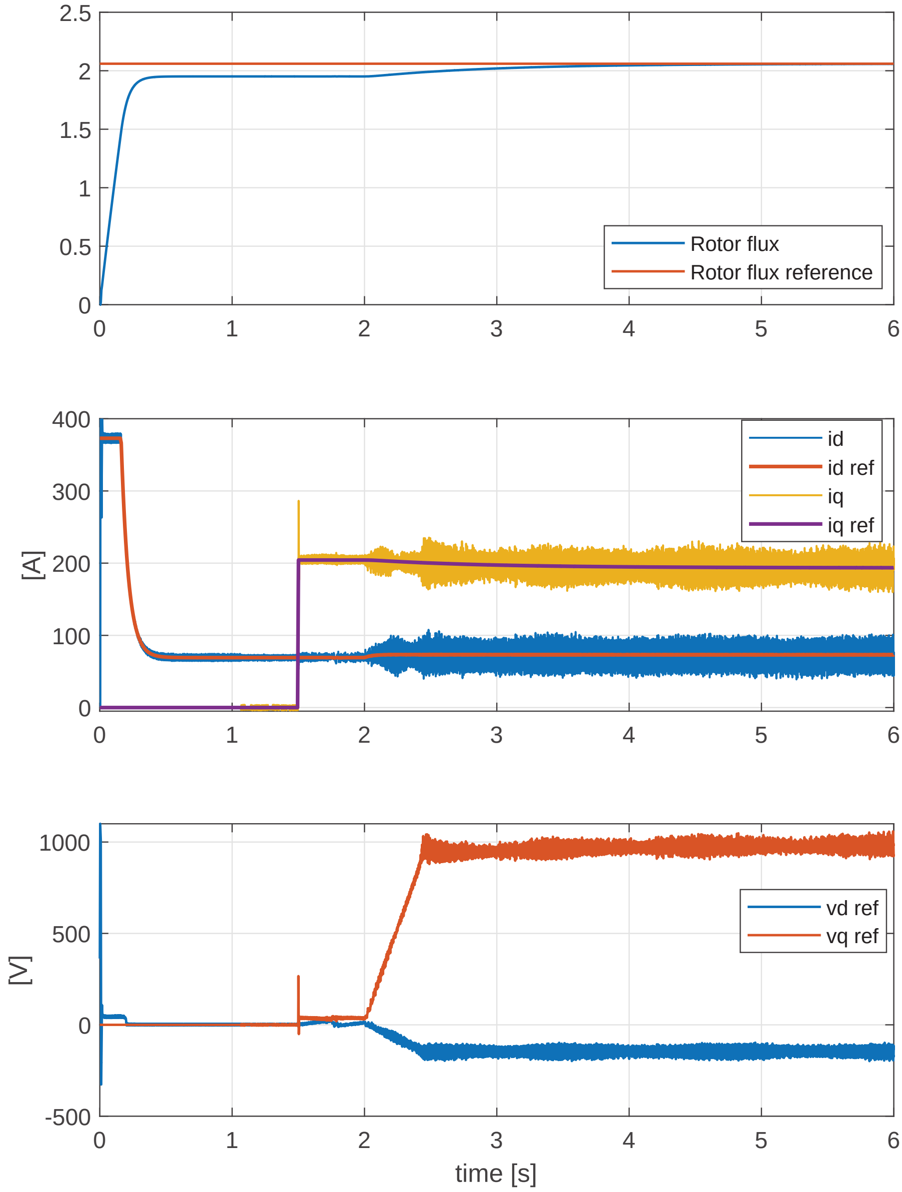

Figure 5.4: Flux, current and voltage references

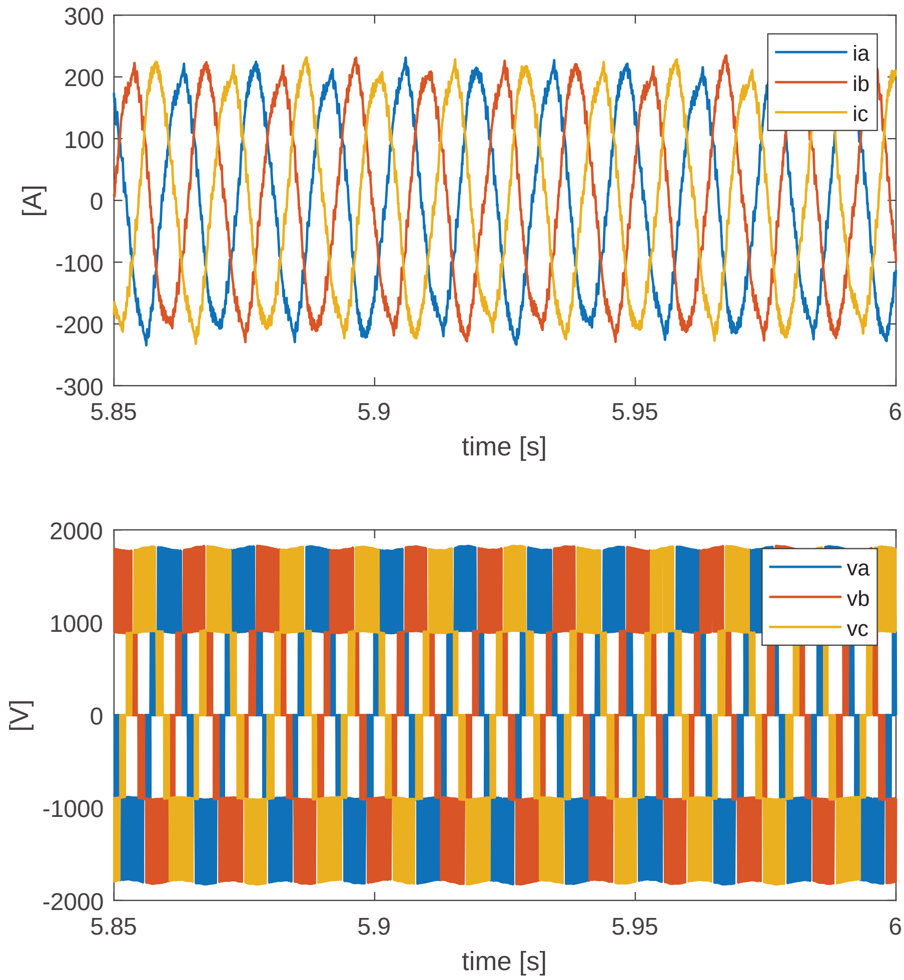

Figure 5.5: Output inverter phase currents and phase to neutral voltages

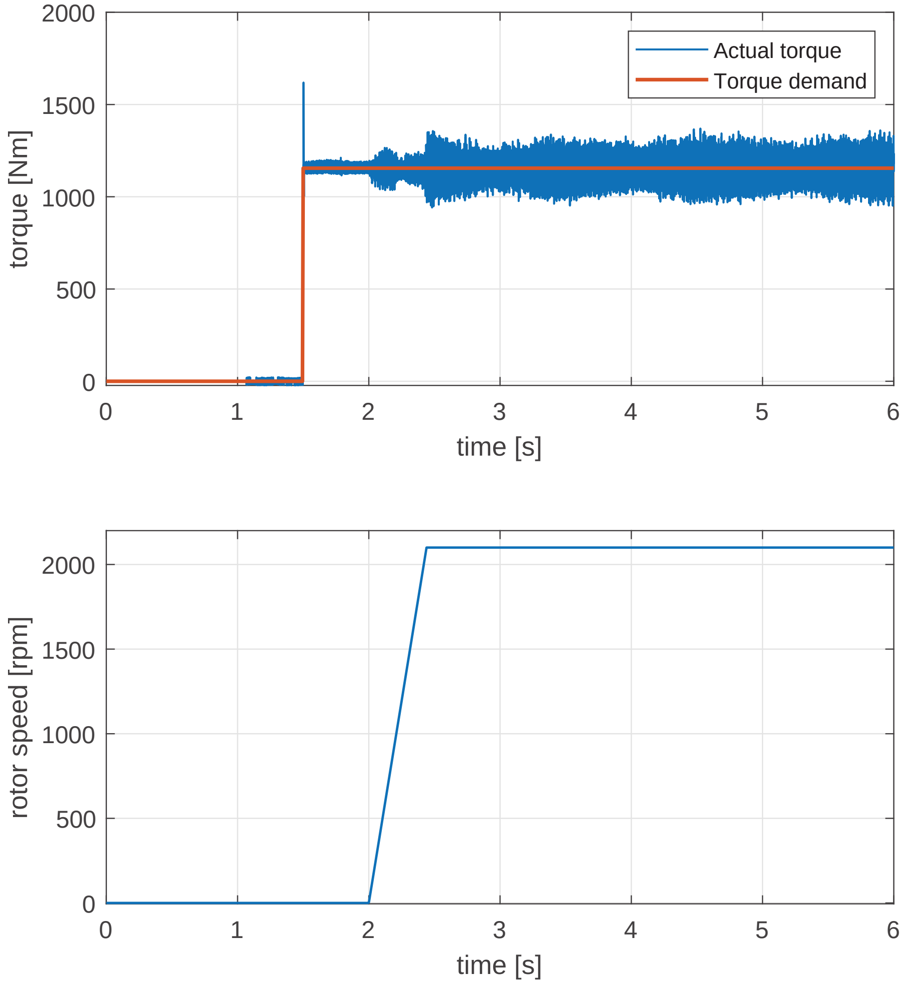

Figure 5.6: Induction machine torque and speed

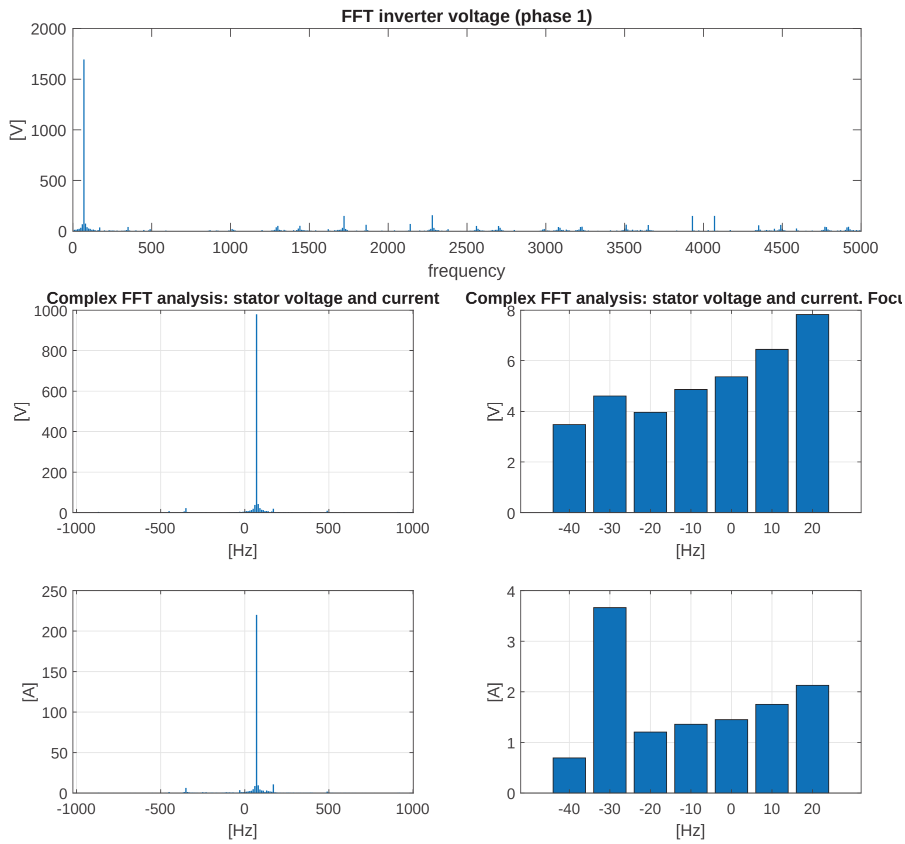

Figure 5.7: FFT analysis of stator voltage and current

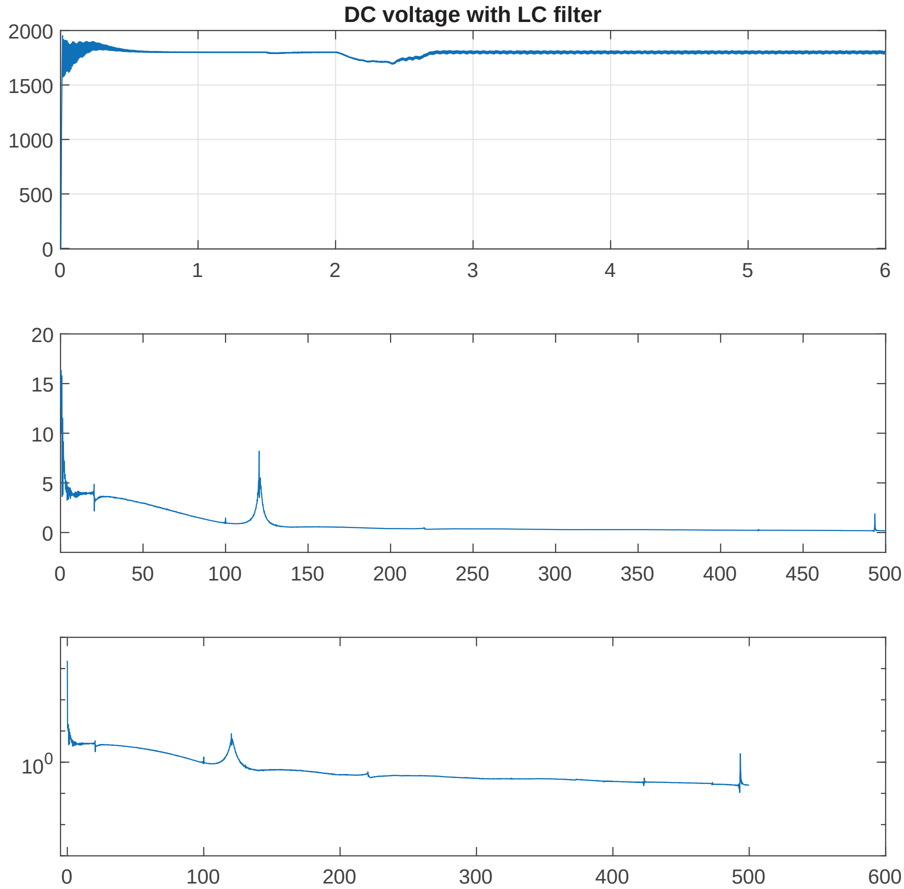

Figure 5.8: DC bus voltage and FFT with filter

this ripple, it was tuned to delate the second harmonic and its removal causes the ripple display, though the rectifier control was very precise.

The harmonic content that is present into the *DC* bus is reported in the harmonic content of the torque as is reported in figure 5.12 and 5.13. Figures 5.14 and 5.15 show the focus of the torque FFT analysis around the second harmonic, the behaviour is similar to the *DC* analysis. Also in this case, the presence of the filter implies no 100 Hz ripple in the spectrum, on the other hand its absence gets the $2f$ torque ripple the most important component on the spectrum. Both FFT of the torque present a ripple around 96 Hz, it may be due combinations amongst inverter and not perfectly clean reference signal.

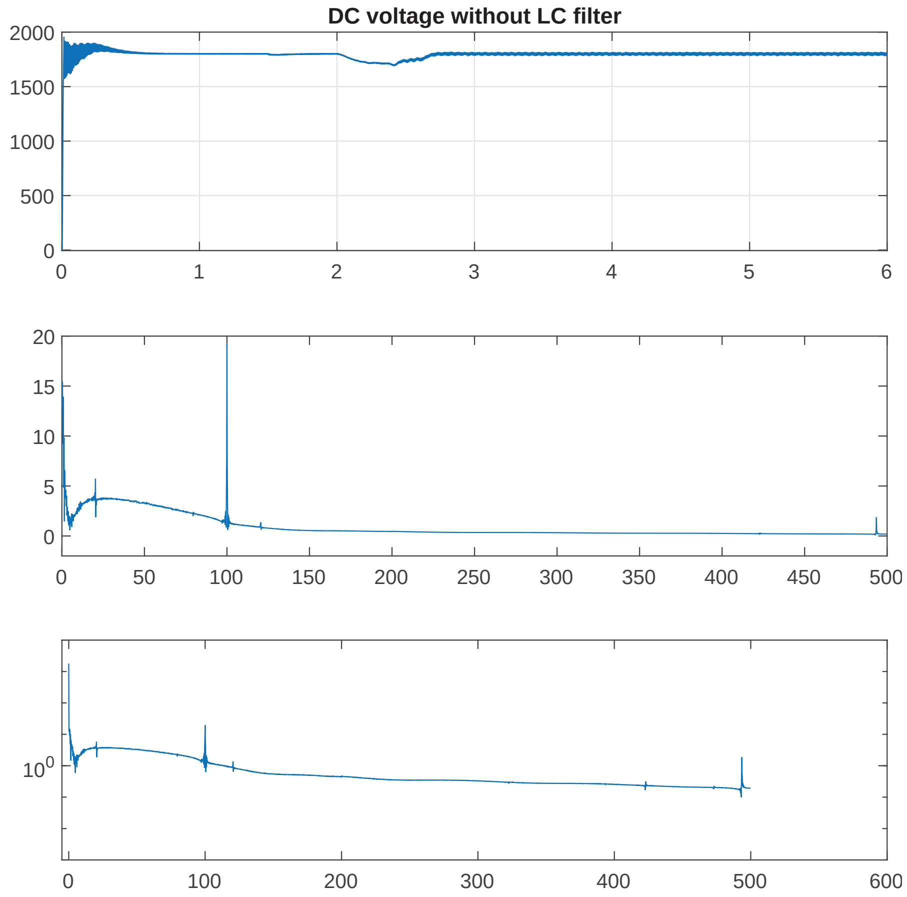

Figure 5.9: DC bus voltage and FFT without filter

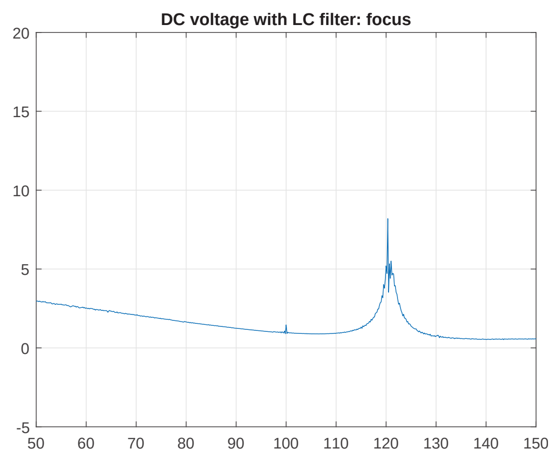

Figure 5.10: FFT DC bus voltage with filter - focus

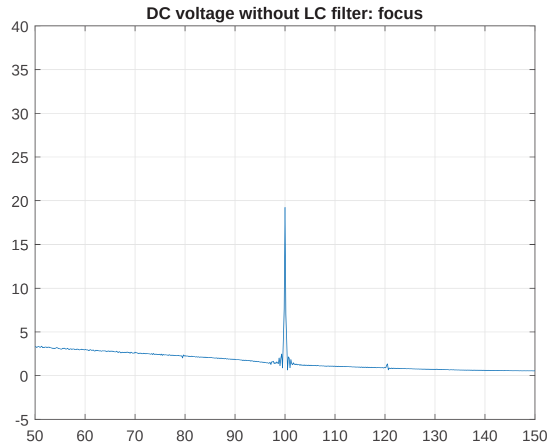

Figure 5.11: FFT DC bus voltage without filter - focus

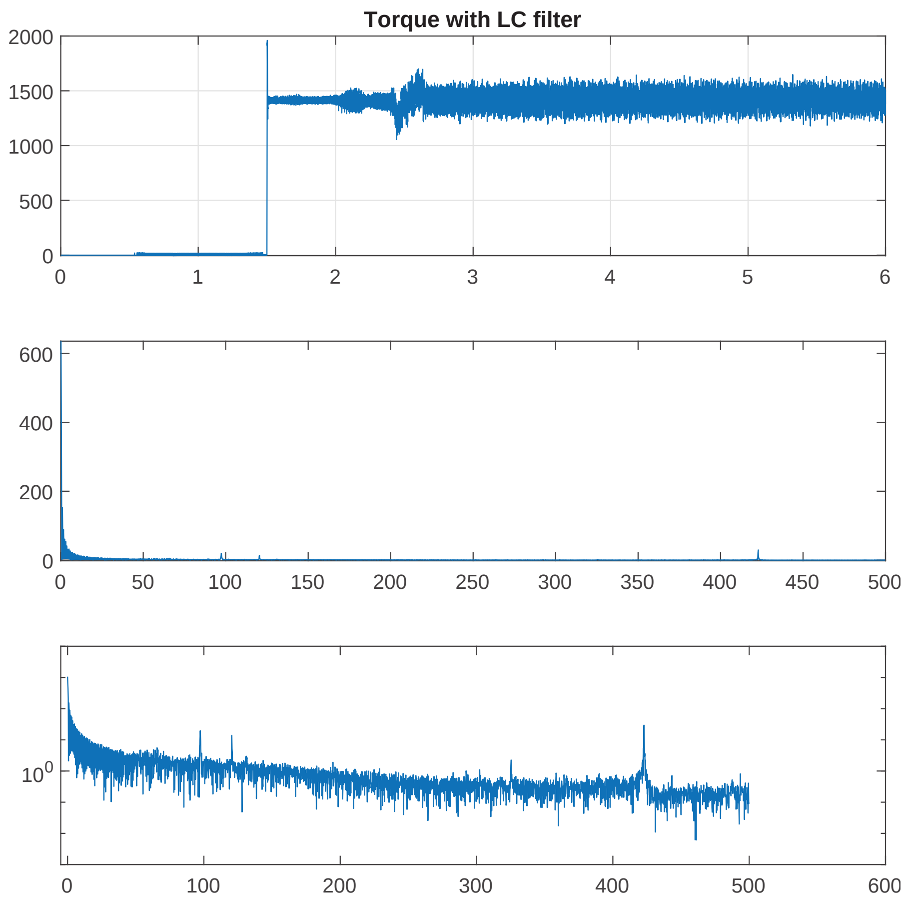

Figure 5.12: Torque and FFT with filter

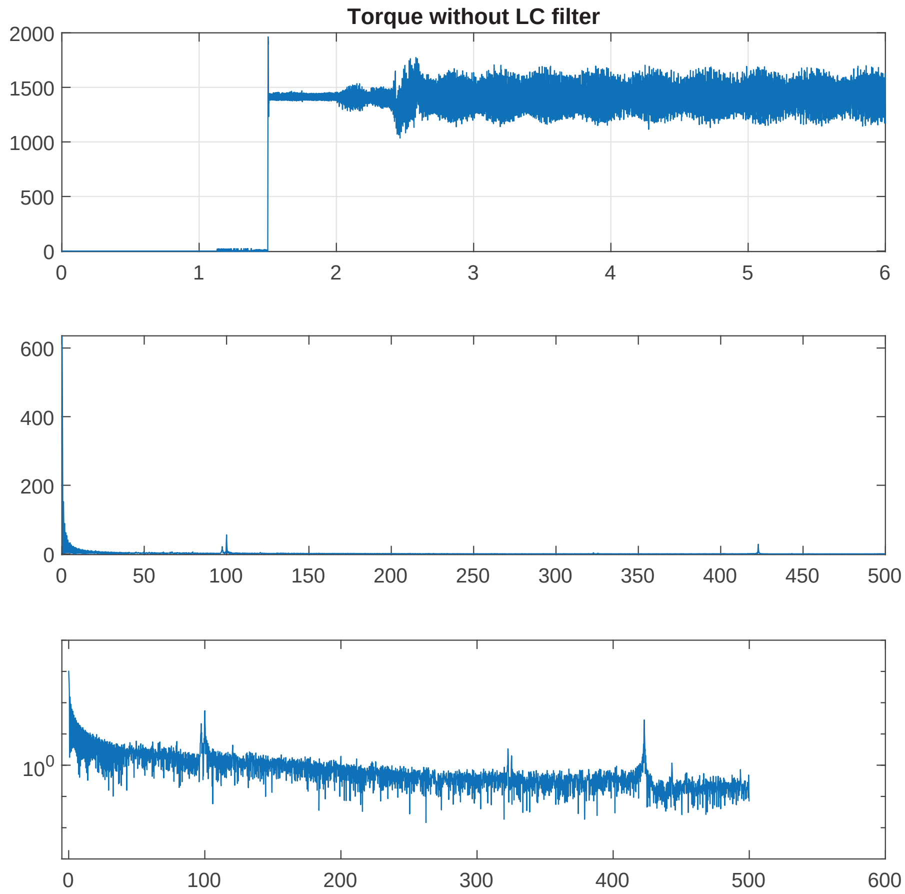

Figure 5.13: Torque and FFT without filter

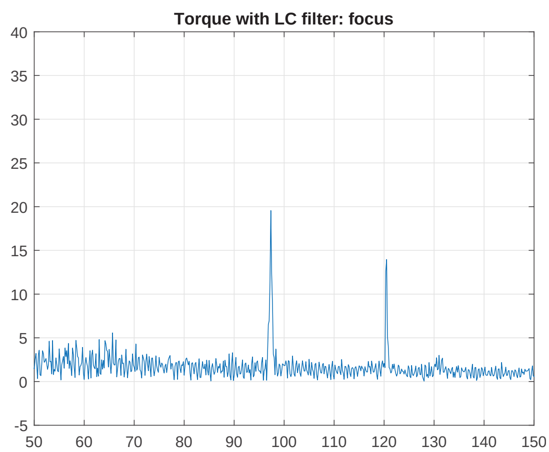

Figure 5.14: FFT torque with filter - focus

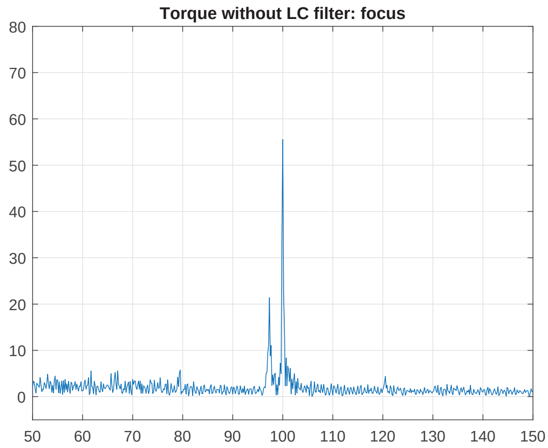

Figure 5.15: FFT torque without filter - focus

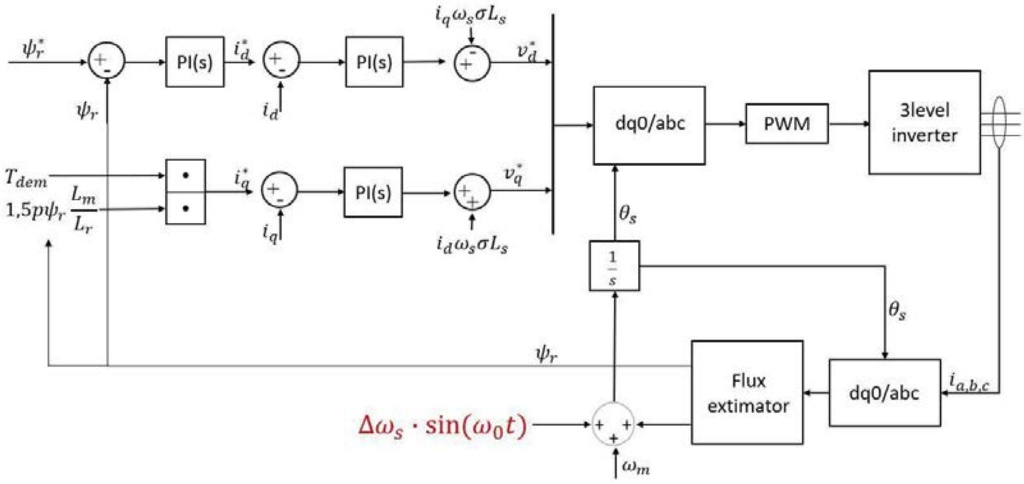

Figure 5.16: Slip injection block diagram

5.3 FREQUENCY INJECTION

In chapter 4, different solutions to reduce the torque ripple have been presented, both using feedback and frequency techniques.

In order to have a better comprehension of the system behaviour and understand how to tune the control, the first part of the study has been focused on a control to reduce the beat effect based on open-loop strategy. The basic idea is the one from the frequency modulation, therefore the switching function has to be modified through frequency modulation. The scheme represented in figure 4.4 at page 30 is modified as represented in figure 5.16.

Chosen an operation condition, an oscillating disturbance (s_{inj}) is added to the slip and then the results are compared to the case without

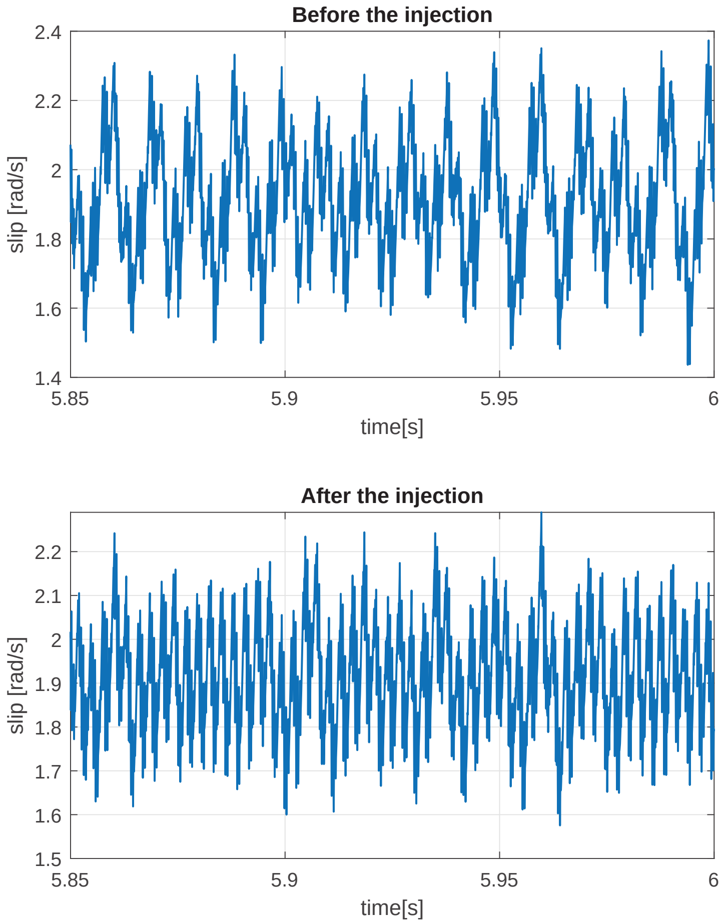

Figure 5.17: Slip without injection (above) and with injection(below)

filter and without injection, in order to see if there is any kind of improvement or understand how to modify s_{inj} to obtain it.

$$s_{inj}(t) = \Delta\omega_s \sin(\omega_0 t + \alpha) \tag{5.3}$$

$\Delta\omega_s$ is the amplitude of this disturbance, ω_0 its frequency and α the phase angle to achieve the synchronization with the actual oscillation of the slip and cancel it. Different values of all variables have been tried for different load and torque conditions.

The first point is the choice related to the disturbance frequency. Considering that the torque ripple appears at 100 Hz, it is logic to inject a slip disturbance at the same frequency. In fact, this injection s_{inj} has an average value equal to zero, but it has to cancel the ripple transmitted from the *DC* link downstream to the motor. The sum of this signal and the actual slip waveform has to bring a constant value. Thanks to this injection it is possible to remove the filter usually used at the *DC* side and to have no ripple at the motor side, as widely discussed in the previous chapters.

Figure 5.17 shows how the slip changes from the case without disturbance injection (above) to the case with it (below). In the first case the 100 Hz harmonic component is evident, in fact if you consider a time interval of 0, 1 s, you can easily count 10 peaks ($T = 1/2f = 1/100 = 0,01$s is the period for the second harmonic). After the disturbance injection, the ripple period is shorter and not easily distinguishable, as it can be seen in the second graph in the same figure. The slip is not constant as wished, but the ripple has high-frequency components which do not cause big issues, the IM presents an inductive behaviour so high-frequency harmonics are not problematic for its proper work.

Simulation tests have confirmed that $\omega_0 = 100$ Hz is the best choice to good results.

5.3.1 *Different torque demand*

In the first part of simulations, the machine speed has been set at 100 Hz and the system has been studied changing the torque demand. Set an amplitude, different simulations have been done changing different α angles. In this way, it was possible to understand which angle could bring the biggest decrease in the ripple. Using the FFT analysis the amplitude and the angle corresponding the *2f* has been taken and plotted in a polar reference frame.

The first case is studied imposing the torque demand equal to $0,9 \cdot T_{rated}$, i.e. 90 % of the rated torque. For example figure 5.18 is obtained setting the amplitude $\Delta\omega_s = 2$ rad/s and changing the phase angle. In the figure the points are numerate and the correspondences are:

1. $\alpha = 0$ rad;
2. $\alpha = \pi/4$ rad:
3. $\alpha = \pi/2$ rad;
4. $\alpha = 3\pi/4$ rad;
5. $\alpha = \pi$ rad;
6. $\alpha = 3\pi/2$ rad.

The one without number is the ripple value without slip injection. The amplitude of the second harmonic without injection and without the filter is 63, 15 Nm, its phase 28, 3 degrees.

Once set the optimal phase angle for the injection, the machine behaviour has been studied with different values of amplitude injections. Results are reported in figure 5.19. The injection that minimizes the ripple effect corresponds to $\Delta\omega_s = 10$ rad/s with a phase shift

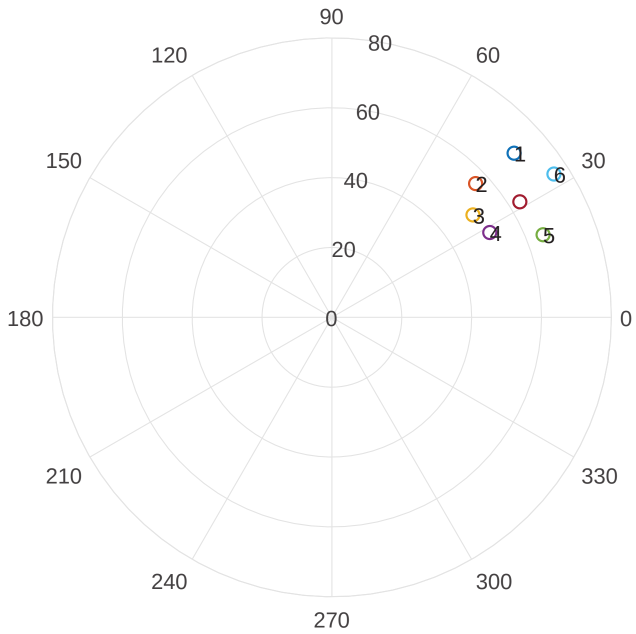

Figure 5.18: Different phase angle in slip injection - 0,9*rated torque case

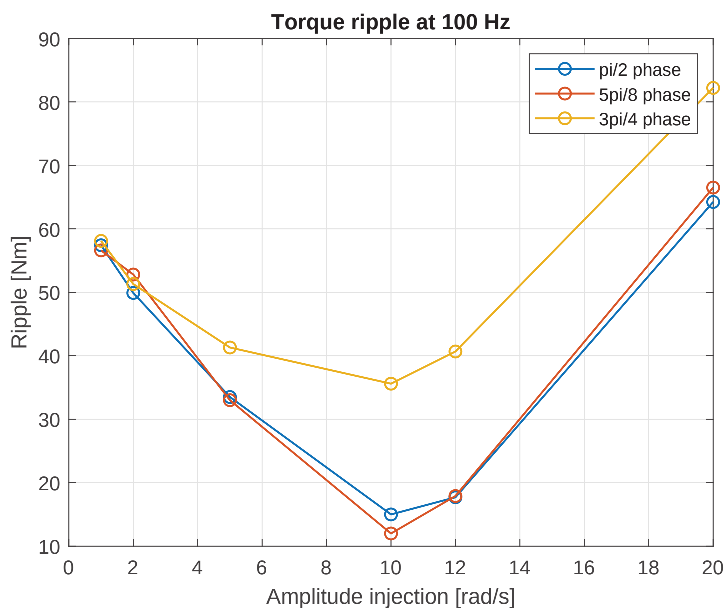

Figure 5.19: Different amplitude in slip injection - 0,9*rated torque case

$\alpha = 5\pi/8$. The ripple decreases to 12 Nm, that is equivalent to a decrease of 80, 99 %.

As said before, the target of this part is to find the correlation between the slip injection needed to decrease the torque ripple and the torque demand required to the machine.

The torque demand now considered is $T = 1,0 \cdot T_{rated}$, i.e. the nominal torque.

Figure 5.20 represents the amplitude and the correspondent phase angle of the 2*f* torque amplitude with fixed $\Delta\omega_s = 10$ rad/s and different phase angles.

1. $\alpha = \pi/4$ rad;
2. $\alpha = 3\pi/8$ rad:
3. $\alpha = \pi/2$ rad;
4. $\alpha = 5\pi/8$ rad;
5. $\alpha = 3\pi/4$ rad;
6. $\alpha = 7\pi/8$ rad.

The one without number is the ripple value without slip injection. It corresponds to a ripple of 112, 6 Nm $\angle 31.61°$.

Set that the optimal injection phase angle is $\alpha = 5\pi/8$, simulations with different amplitudes have been done. Results are represented in figure 5.21. In this case, the minimum is achieved with $\Delta\omega_s = 10$ rad/s. The ripple decreases to 9, 45 Nm with $\angle 31.61°$. Therefore the best improvement, in this case, is obtained injecting $s_{inj} = 10 \sin[(2\pi 100)t + 5\pi/8]$, the ripple decreases by 91%.

Following the same logic method, the torque $T = 0,7 \cdot T_{rated}$ is studied.

As the previous cases, some simulations have been run to understand what is the best phase angle α to minimize the torque ripple.

In this case, the ripple in the worst case is equal to 52, 5 Nm with 90 degrees of phase shift on FFT corresponding to the second harmonic. The other tested angles are:

1. $\alpha = \pi/4$ rad;
2. $\alpha = 3\pi/8$ rad:
3. $\alpha = \pi/2$ rad;
4. $\alpha = 5\pi/8$ rad;
5. $\alpha = 3\pi/4$ rad.

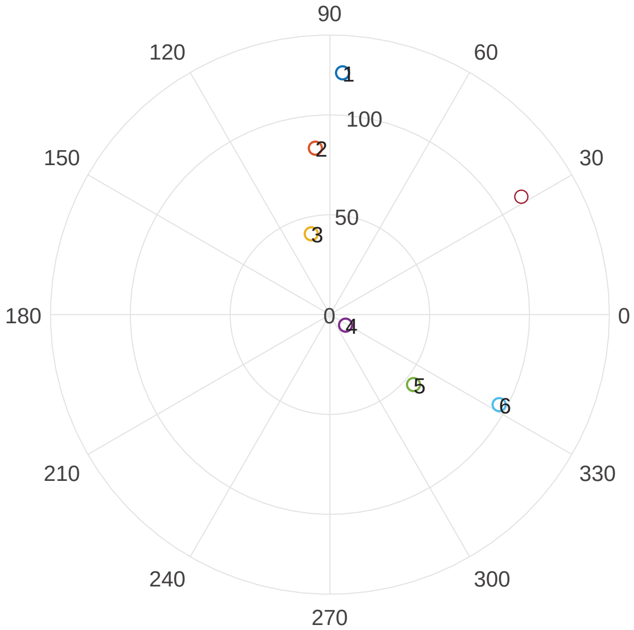

Figure 5.20: Different phase angle in slip injection - 1,0*rated torque case

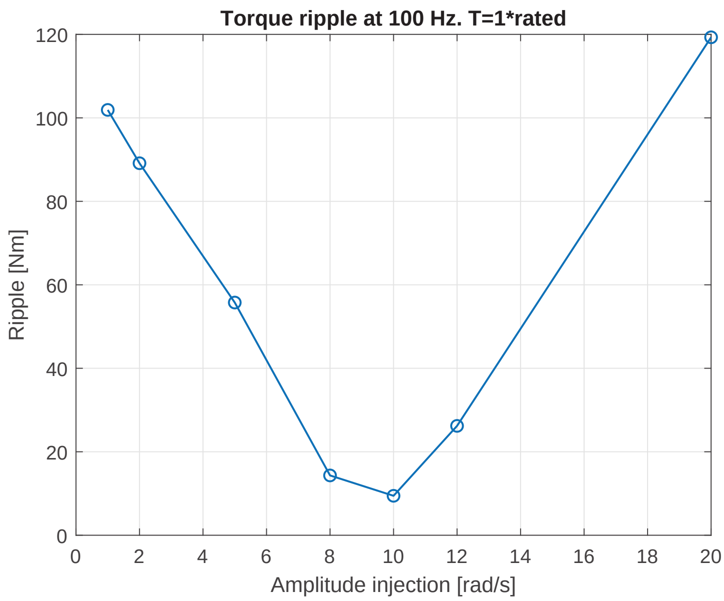

Figure 5.21: Different amplitude in slip injection - 1,0*rated torque case

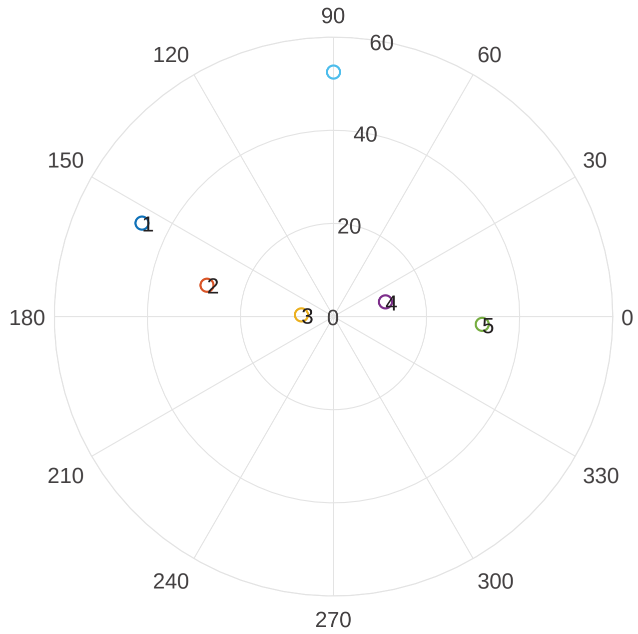

Figure 5.22: Different phase angle in slip injection - 0,7*rated torque case

The one without number is the ripple value without slip injection.

Figure 5.22 shows how the torque ripple changes with different angles and fixed amplitude $\Delta\omega_s = 8$ rad/s.

Figure 5.23 shows how the torque ripple changes with different amplitudes. In this case the best improvement is obtained injecting $s_{inj} = 8\sin[(2\pi 100)t + \pi/2]$. There is a percentage decrease equal to $86,86\,\%$ imposing $\Delta\omega_s = 8$ rad/s and $\alpha = \pi/2$. The ripple decreases from $52,5$ Nm to $6,9$ Nm after the injection.

The torque $T = 0,4 \cdot T_{rated}$ is now studied.
The first step is finding the optimal injection angle, the one that can minimize the $2f$ torque ripple. As usual, an amplitude is fixed ($\Delta\omega_s = 8$ rad/s) and different phase angles are tried running different simulations. Referring to figure 5.24, these angles are:

1. $\alpha = \pi/4$ rad;
2. $\alpha = 3\pi/8$ rad:
3. $\alpha = \pi/2$ rad;
4. $\alpha = 5\pi/8$ rad;
5. $\alpha = 3\pi/4$ rad;
6. $\alpha = 7\pi/8$ rad.

The one without number is the ripple value without slip injection.

Without injection the ripple is equal to $11,62$ Nm $\angle 126.33°$. In the same figure, the amplitude and correspondent phase angles are reported in the polar plot.

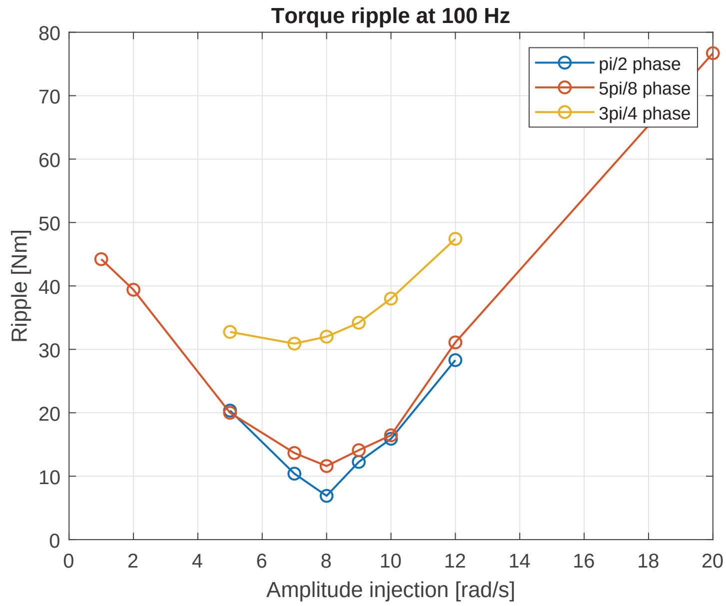

Figure 5.23: Different amplitude in slip injection - 0,7*rated torque case

Figure 5.25 represents the behaviour of the system changing the amplitude of slip injection. The ripple decreases of 81,4 % with $s_{inj} = 4\sin[(2\pi 100)t + \pi/2]$ injection. From 11,62 to 2,16 Nm after the injection.

The last studied case is the one with torque demand $T = 0,1 \cdot T_{rated}$. In this case, the ripple values are small considering both the case with injection and without it. In fact, the ripple amplitude without filter and without injection is equal to 2,965 Nm, phase angle $-178°$. Figure 5.26 shows that in some case the difference between the presence or not of the injection does not make any difference (point 1 and 2). Anyhow, the following angles have been tested to find the optimal one, fixing the amplitude $\Delta\omega_s = 2$ rad/s.

1. $\alpha = \pi/4$ rad;
2. $\alpha = 3\pi/8$ rad:
3. $\alpha = \pi/2$ rad;
4. $\alpha = 5\pi/8$ rad;
5. $\alpha = 3\pi/4$ rad;
6. $\alpha = 7\pi/8$ rad.

The one without number is the ripple value without slip injection.

Once fixed that the optimal angle corresponds to $5\pi/8$, the effects of different amplitudes have been compared as it is reported in figure 5.27. In this case the best improvement is obtained injecting $s_{inj} =$

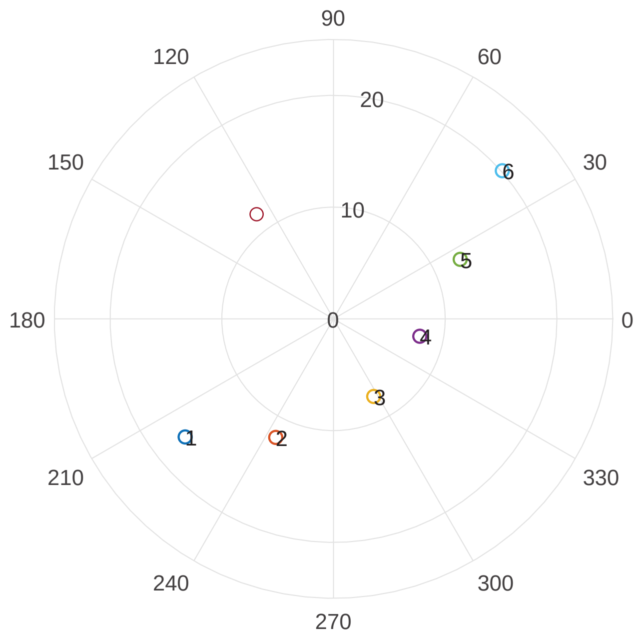

Figure 5.24: Different phase angle in slip injection - 0,4*rated torque case

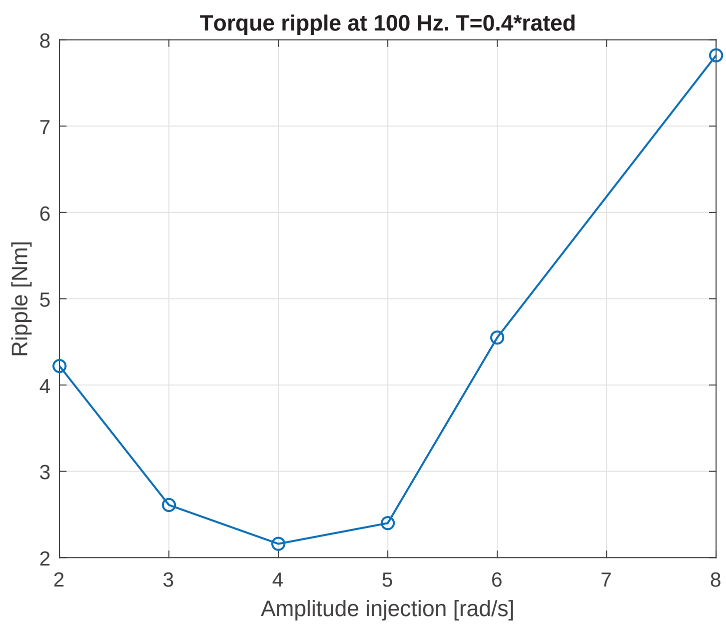

Figure 5.25: Different amplitude in slip injection - 0,4*rated torque case

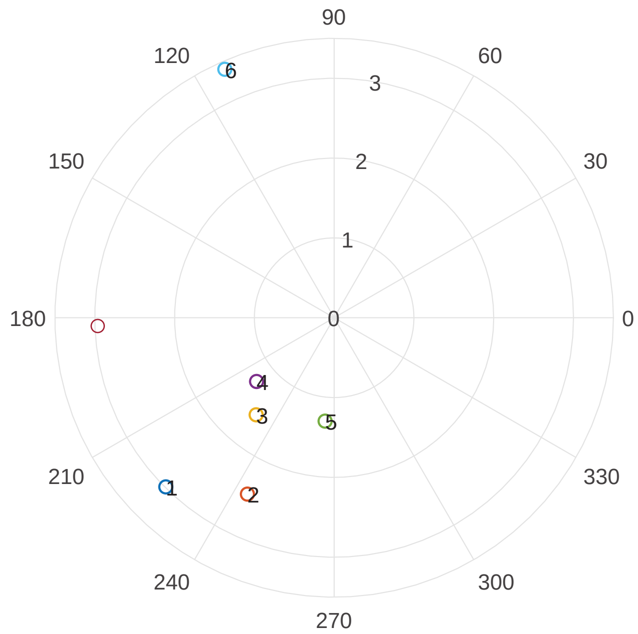

Figure 5.26: Different phase angle in slip injection - 0,1*rated torque case

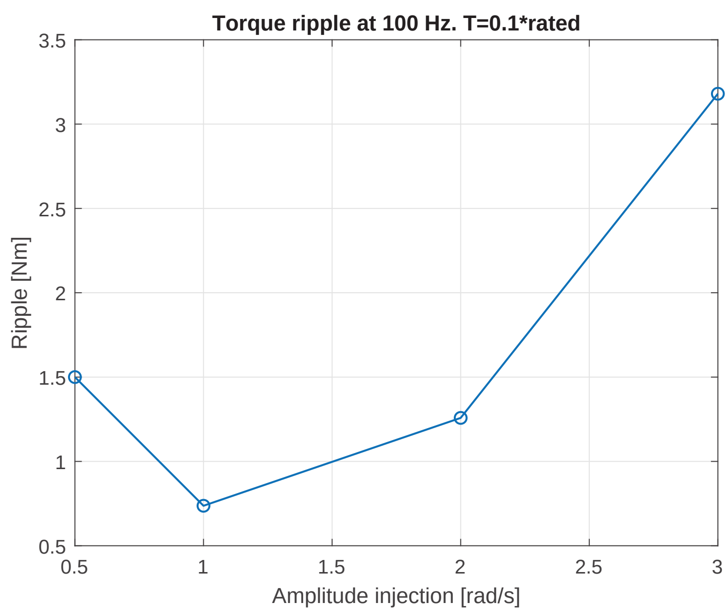

Figure 5.27: Different amplitude in slip injection - 0,1*rated torque case

$1\sin[(2\pi 100)t + 5\pi/8]$. The new ripple is $0,737$ Nm, with a percentage decrease of the ripple of $75,14\,\%$.

In order to understand how the system evolves and how to adjust the slip injection, other simulations have been run to find the optimal injection. The torque demand has been changed with steps of value $0,1 \cdot T_{rated}$. Table 5.1 summarizes the results.

Figure 5.28 represents the amplitude and the phase angle for slip injection with different torque demand in a visual and immediate form. The first row represents the amplitude $\Delta\omega_s$ needed to obtain the best improvement in the behaviour of the machine. It is clear that there is a linear trend between the torque required and the amplitude value needed. Equation (5.4) could describe this trend.

$$\Delta\omega_s = \frac{10 \cdot T_{demand}}{T_{rated}} \tag{5.4}$$

In the same figure, the second row represents the phase angle for the slip injection, apparently there is not a relationship between torque demand and α. It could be related to the behaviour of the machine with that particular torque demand and load machine speed.

Figure 5.29 compares the ripple value before and after the injection of the slip oscillation. The value that corresponds to the second harmonic is normalized on the demand value, i.e. the ripple is divided by the torque demand both with disturbance injection and without it. In this way, it is possible to compare results with different machine behaviour. It is evident that the ripple content is larger with higher torque demand value before the injection, but after it the ripple is 1% (or less) of the main component. The slip injection improves a lot the behaviour of the system.

Figure 5.30 shows the percentage decrease of the ripple after the slip injection. Consider that the percentage decrease is less reliable for low torque demand because the absolute ripple is small, though the relative ripple value is big.

5.3.2 *Different machine speed*

In the previous section, the effect of different slip injections has been studied changing the torque demand with fixed rotor speed. Now, the torque demand has been fixed, $T_{demand} = 0,9 \cdot T_{rated}$, and the rotor speed has been changed between 50 Hz and 100 Hz. Considering that the nominal rotor speed is 50 Hz, for higher load speed it is necessary to use field weakening techniques and so to use flux command lower than the rated one.

The first test is considering the rated rotor speed and the rated rotor flux. The IM without *LC* filter at the *DC* bus side and without slip

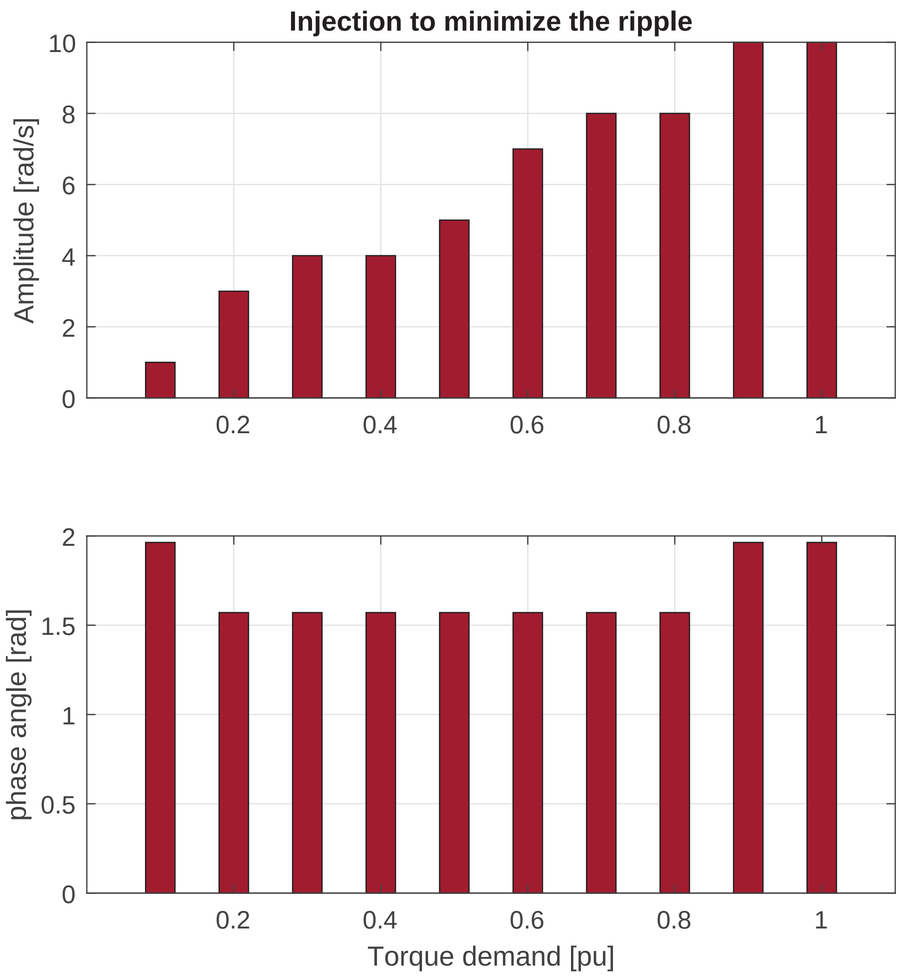

Figure 5.28: Slip injection - amplitude and angle

Table 5.1: Torque ripple with different torque demand - final report

Torque value	Ripple [Nm] Before	After	Slip injection	% decrease
$0,1 \cdot T_r$	2.965	0.737	$1\sin(\omega_0 t + \frac{5\pi}{8})$	75,14
$0,2 \cdot T_r$	7.677	1.64	$3\sin(\omega_0 t + \frac{\pi}{2})$	78.64
$0,3 \cdot T_r$	10.14	1,48	$4\sin(\omega_0 t + \frac{\pi}{2})$	85,40
$0,4 \cdot T_r$	11,62	2,16	$4\sin(\omega_0 t + \frac{\pi}{2})$	81,41
$0,5 \cdot T_r$	20,3	4,38	$5\sin(\omega_0 t + \frac{\pi}{2})$	78,42
$0,6 \cdot T_r$	33,7	2	$7\sin(\omega_0 t + \frac{\pi}{2})$	94,01
$0,7 \cdot T_r$	52,5	6,9	$8\sin(\omega_0 t + \frac{\pi}{2})$	86,86
$0,8 \cdot T_r$	60,08	12,28	$8\sin(\omega_0 t + \frac{\pi}{2})$	79,56
$0,9 \cdot T_r$	63,15	12	$10\sin(\omega_0 t + \frac{5\pi}{8})$	80,99
$1,0 \cdot T_r$	112,6	9,45	$10\sin(\omega_0 t + \frac{5\pi}{8})$	91,61

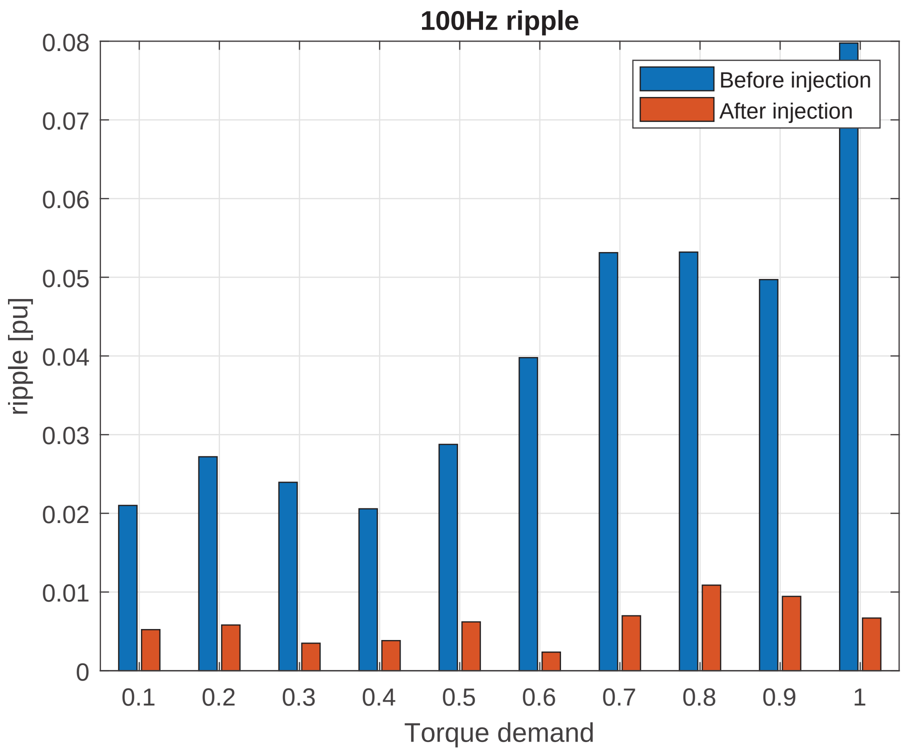

Figure 5.29: 2f ripple - before and after the slip injection

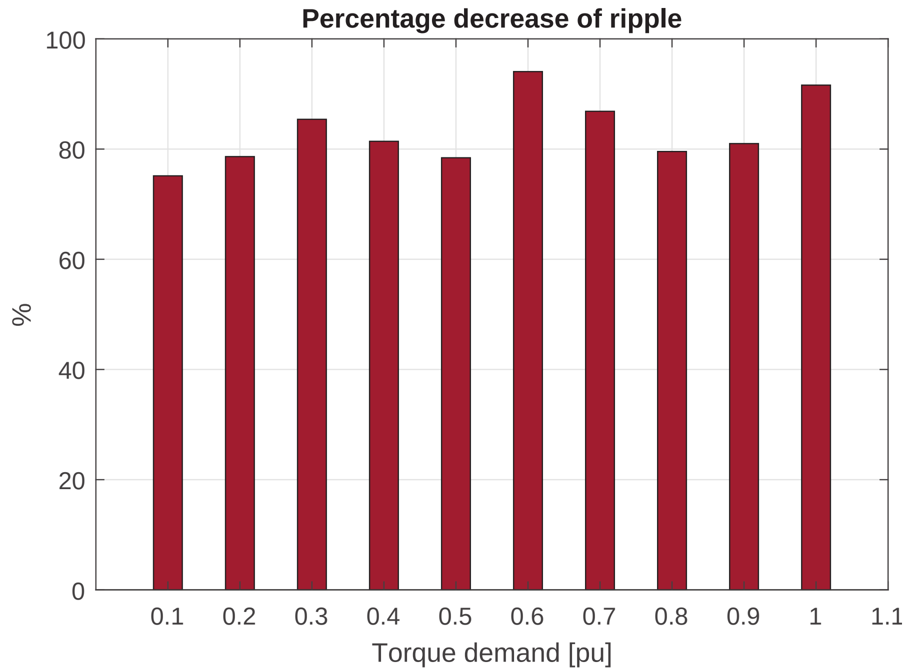

Figure 5.30: Percentage decrease of the ripple

injection presents a torque ripple at the frequency $f = 100$ Hz equal to $108, 55$ Nm. Figure 5.31 presents the torque ripple after different slip injections: in the general slip expression $s_{inj} = \Delta\omega_s \sin(\omega_0 t + \alpha)$, different amplitudes and phase angles have been used. In particular, $\Delta\omega_s = \{5; 8; 9; 10; 11; 15\}$ rad/s and $\alpha = \{3\pi/8; \pi/2; 5\pi/8\}$ radiants. The optimal injection is $s_{inj} = 10 \sin(\omega_0 t + \pi/2)$ which produces a ripple of $10, 24$ Nm, corresponding to a decrease of $90, 57\%$ of the ripple problem.

The second test on the motor behaviour is made setting the machine load speed at 60 Hz and using the flux reference $\lambda_{req} = 0.83 \cdot \lambda_{rated}$, from equation (5.2). Before injecting s_{inj}, the torque ripple is $106, 3$ Nm, after the optimal one, the ripple is reduced to $5, 5$ Nm, that is the $94, 83\%$ percent decrease. The best result is obtained with a disturbance injection with $\Delta\omega_s = 10$ rad/s amplitude and $\alpha = \pi/2$ rad phase angle. As it is represented in figure 5.32, the optimal injection has been found after different test both for amplitude and phase angle.

The results shown in figure 5.33 have been obtained with rotor speed set at 70 Hz and rotor flux $\lambda_{req} = 0, 71 \cdot \lambda_{rated}$. In this case the amplitude has been changed as $\Delta\omega_s = \{5; 9; 10; 11; 15\}$ rad/s and phase angle $\alpha = \{3\pi/8; \pi/2; 5\pi/8\}$ radiants. Before the slip alteration, the torque ripple is $88, 9$ Nm, but after it, a percentage decrease equal to $89, 64\%$ can be obtained. The torque ripple goes to $9, 21$ Nm after the injection with 10 rad/s amplitude and $\pi/2$ phase angle.

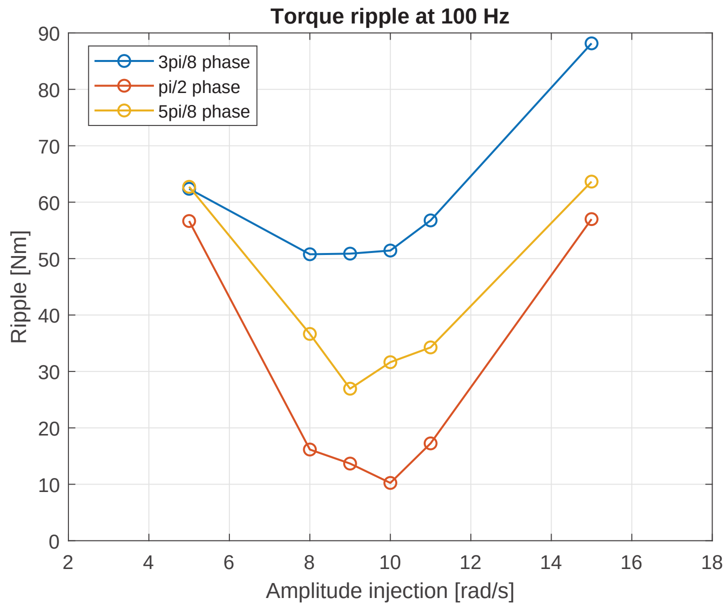

Figure 5.31: Different amplitude and phase angle in slip injection - 50 Hz machine speed

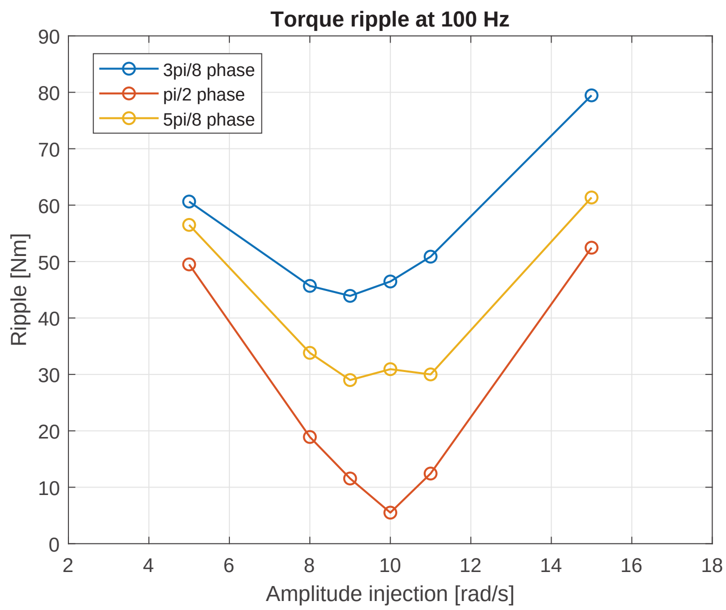

Figure 5.32: Different amplitude and phase angle in slip injection - 60 Hz machine speed

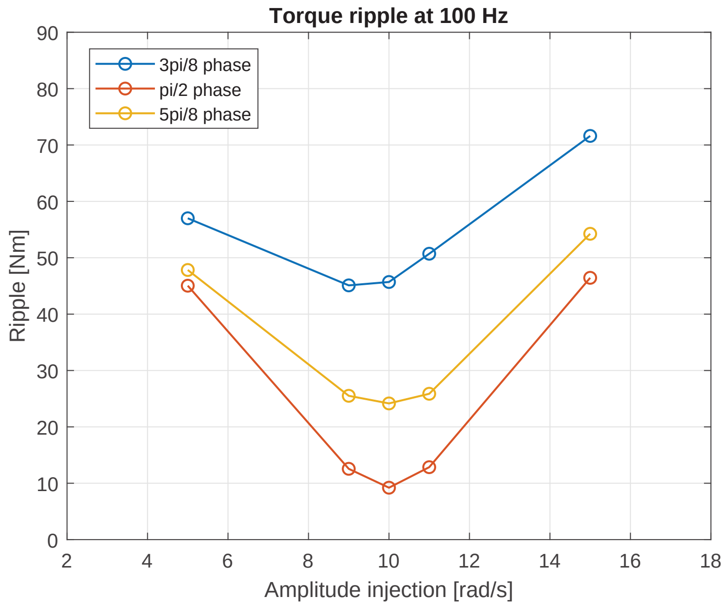

Figure 5.33: Different amplitude and phase angle in slip injection - 70 Hz machine speed

When the rotor speed is set $\omega_r = 80$ Hz, the rotor flux has to be imposed equal to $0,625 \cdot \lambda_{rated}$, according to the weakening flux technique. Figure 5.34 shows different torque ripples changing disturbance injection conditions s_{inj}, from equation (5.3).
Before the injection, the $2f$ ripple is equal to $93,3$ Nm, after the slip modification the ripple is reduced to $17,47$ Nm, with a decrease of $81,28\%$. The optimal injection is $s_{inj} = 9\sin(\omega_0 t + \pi/2)$.

The case with rotor speed set at 90 Hz and rotor flux equal to $0,54 \cdot \lambda_{rated}$ is studied and results are reported in figure 5.35. The $2f$ torque ripple is $68,67$ Nm without harmonic filter and with no disturbance injection. This value can be improved with s_{inj} injection characterized by 10 rad/s amplitude and $\pi/2$ phase angle. The ripple is $10,8$ Nm after the injection, the percentage decrease is equal to $84,27\%$.

The last case is the one with 100 Hz rotor speed and rotor flux $\lambda_r = 0,475 \cdot \lambda_{rated}$. In this case, the ripple torque before the injection is 63 Nm and can be improved to $11,3$ Nm. This result is achieved through an injection $s_{inj} = 10\sin(\omega_0 t + 5\pi/8)$. The ripple decreases by $82,06\%$ in this case.

Table 5.2 summarises all the studied cases, comparing torque ripple before and after slip disturbance injection.

Figure 5.37 represents the optimal amplitude and phase angle for the injection s_{inj} for each load speed. It is evident that there are no big differences in the injections changing the rotor speed, the optimal amplitude is more or less stable and so the phase angle. This is different from the behaviour of the optimal injection achieved from

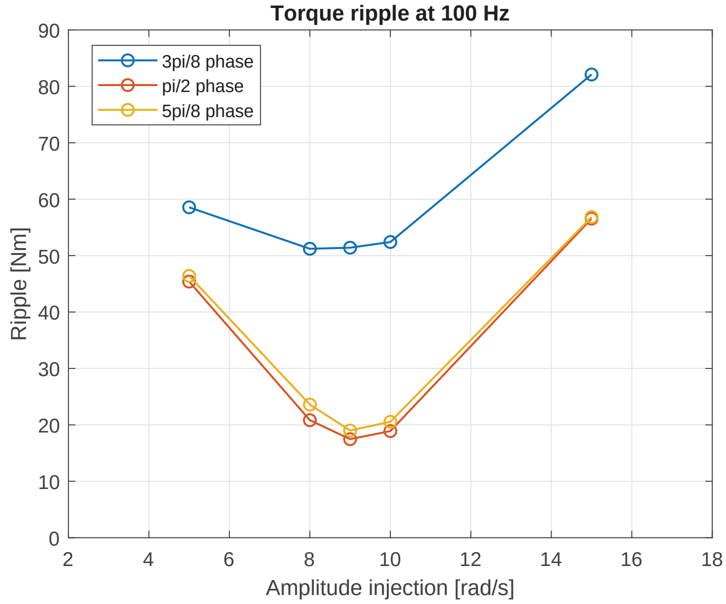

Figure 5.34: Different amplitude and phase angle in slip injection - 80 Hz machine speed

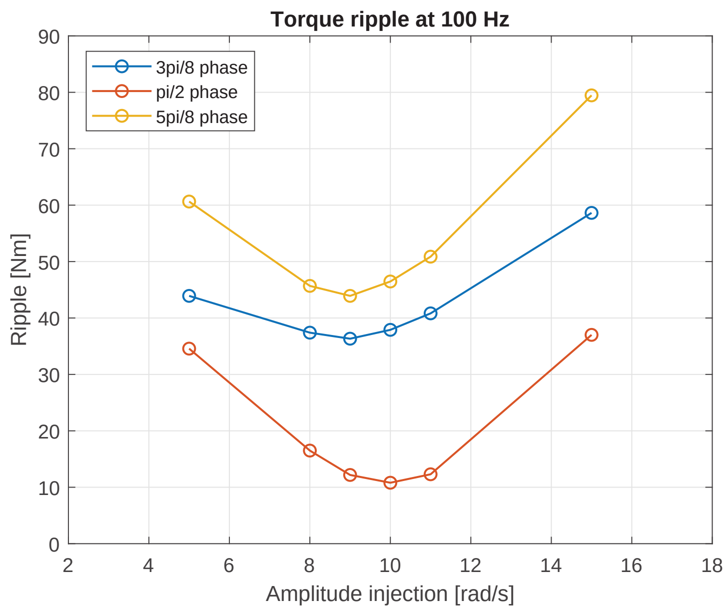

Figure 5.35: Different amplitude and phase angle in slip injection - 90 Hz machine speed

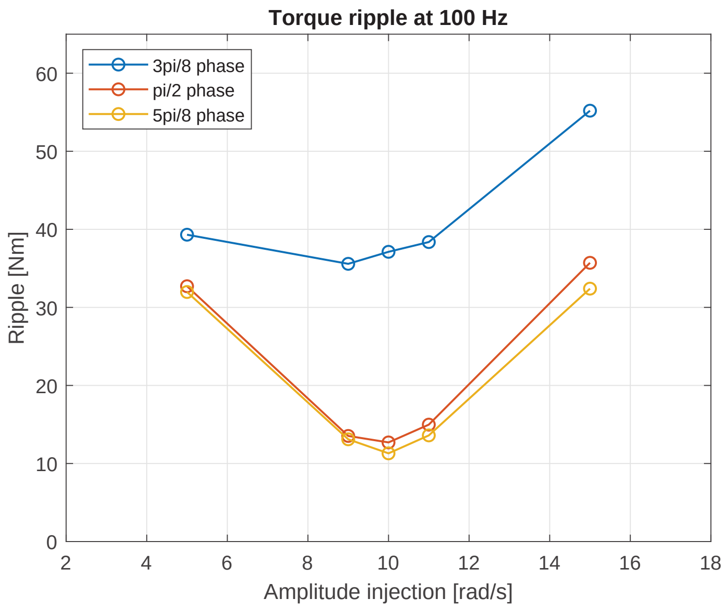

Figure 5.36: Different amplitude and phase angle in slip injection - 100 Hz machine speed

Table 5.2: Torque ripple with different load speed - final report

Speed value [Hz]	Ripple [Nm] Before	Ripple [Nm] After	Slip injection	% decrease
50	108,55	10,24	$10\sin(\omega_0 t + \frac{\pi}{2})$	90,57
60	106,3	5,5	$10\sin(\omega_0 t + \frac{\pi}{2})$	94,83
70	88,9	9,21	$10\sin(\omega_0 t + \frac{\pi}{2})$	89,64
80	93,3	17,47	$9\sin(\omega_0 t + \frac{\pi}{2})$	81,28
90	68,67	10,8	$10\sin(\omega_0 t + \frac{\pi}{2})$	84,27
100	63	11,3	$10\sin(\omega_0 t + \frac{5\pi}{8})$	82,06

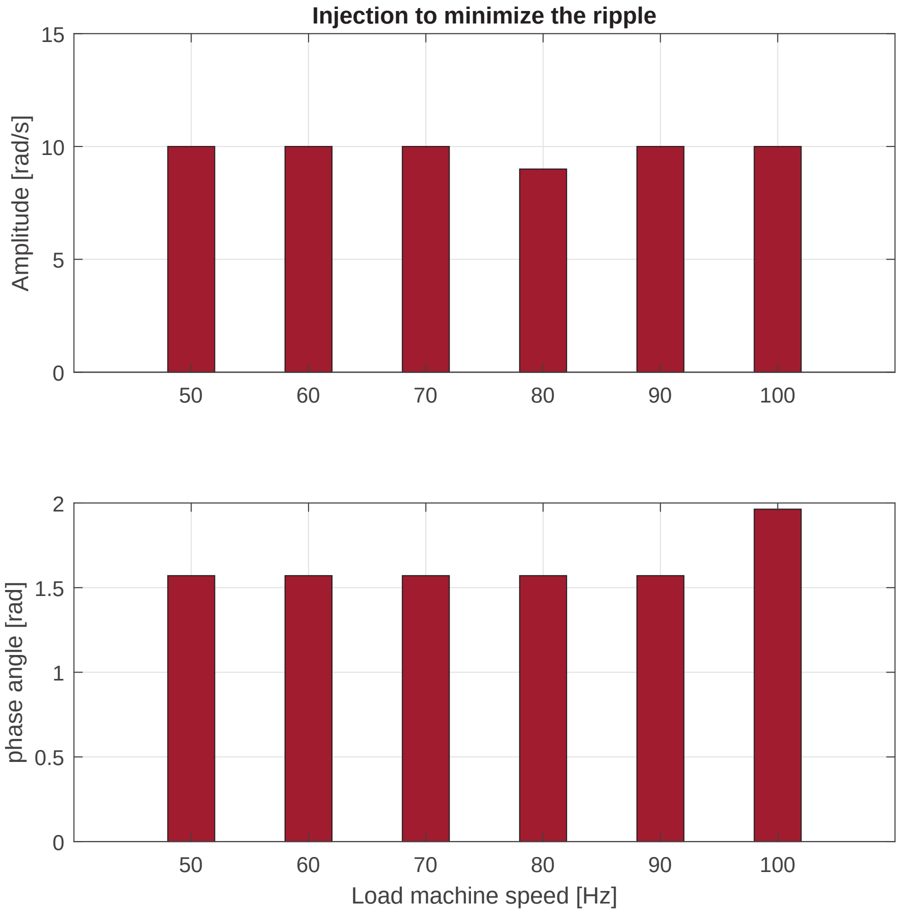

Figure 5.37: Different amplitude and phase angle in slip injection for different machine speed

figure 5.28 with different torque demand. However, considering that the torque demand was fixed $T_{dem} = 0,9 \cdot T_{rated}$ during the studying with different load machine speed, the injection amplitude is coherent with results obtained in the previous section. In fact, the injection needed for $0,9 \cdot T_{rated}$ from table 5.1 is 10 rad/s that is exactly what results from the study with different speeds.

Unlike the previous case, where the system has been studied with different values of torque demand, the percentage decrease is not constant with different conditions. With bigger values of load speed the torque ripple is lower and so it is the percentage decrease after the optimal injection. This effect is shown in figure 5.38, $2f$ harmonic of torque ripples with different conditions are normalized by the value of torque demand, both without and with injection. The torque ripple before the injection decreases with the rotor speed, while after the injection it is almost stable with different conditions. This means that the improvement due to s_{inj} gets worse as the speed increases, as it can be seen in figure 5.39 and read in table 5.2.

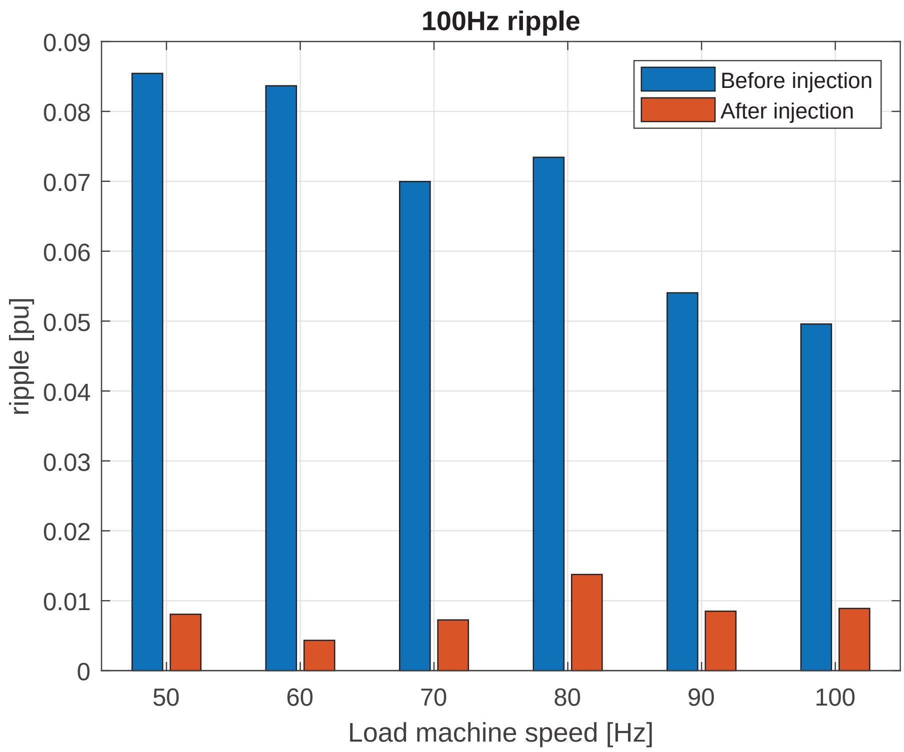

Figure 5.38: Torque ripple before and after slip injection

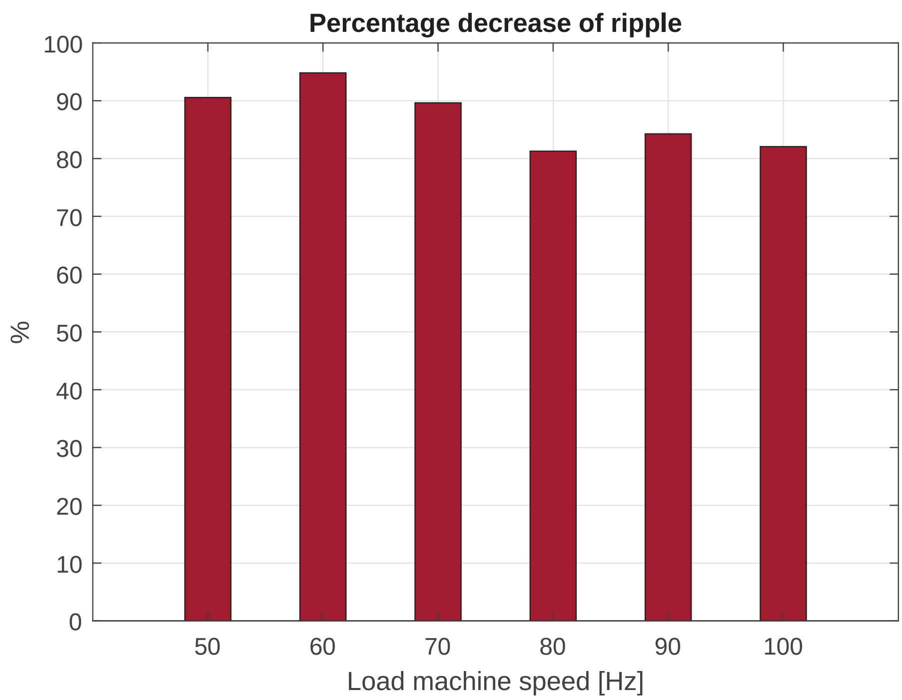

Figure 5.39: Percentage decrease due to slip injection

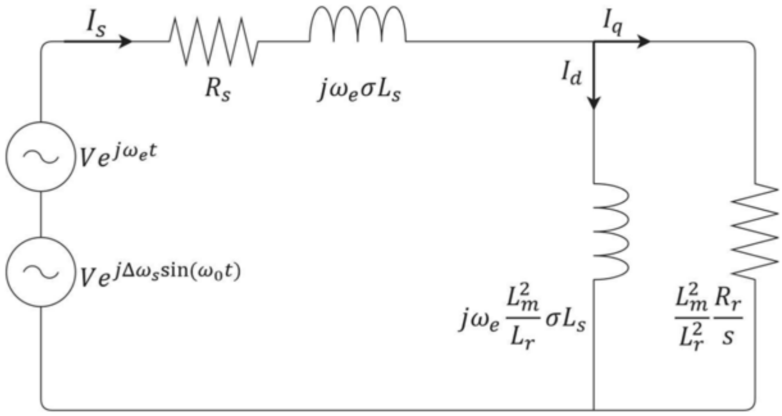

Figure 5.40: Percentage decrease due to slip injection

5.4 considerations on injection's phase angle

The biggest problem of this open-loop analysis is the method to understand what is the optimal angle α to put into disturbance injection $s_{inj} = \Delta\omega_s \sin(\omega_0 t + \alpha)$ to have the best reduction on the torque ripple.

It is well established that the *2f* oscillation from the *DC* link (which comes from the single-phase rectifier, as already said) causes an isofrequency ripple on the motor reference and so on the current and on the torque. Therefore if everything is coming from the *DC* link voltage, it is reasonable to assume that the angle of the pulsation that you get in the torque is somehow related to the angle of the oscillation of the *DC* link voltage.

In order to have a better comprehension of the problem, a comparison between simulation results and a simplified machine model is proposed.

The second harmonic impedance of the machine can be deduced from i_{dq} and v_{dq} values, in fact the amplitude corresponds to the ratio between the 100 Hz component of the FFT of v_{dq} and the 100 Hz component of the FFT of i_{dq}, while the angle is the difference of angles from v_{dq} and i_{dq} FFT analysis. These values are available from the simulations done for the previous analysis.

The second term of comparison is the equivalent model of the machine studied using the superposition of effects method, see the figure 5.40. Using this scheme and the equations that rule the IM, it is possible to achieve the impedance and torque for the simplified model supplied by fundamental voltage and a voltage waveform similar to the disturbance injection.

Once results from both methods are obtained, the comparison between them could help to understand how to obtain a generalized method to have the optimal phase injection angle.

This argument is left to be analysed in the future.

6 CONCLUSIONS AND FUTURE DEVELOPMENTS

It can be said that the creating of a well working control system has taken more time than the expected. It is not a big issue because the Simulink model has been deeply analysed and tested, but this has subtracted time to a complete study on the algorithm to remove the torque ripple without the *DC* link filter.

Results from the control study have been successful and the use of three-level inverter brought many advantages for the harmonic distortion and the power factor, as reported in the chapter with simulation results and in the appendix where current and voltage behaviours from two-level and three-level inverter are reported.

Although the algorithm solutions proposed on the bibliography seemed easy to implement and to adapt to the model, open-loop studies simulations have been preferred to better understand how to adapt the proposals and what is the best improvement achievable. After many tests with different working conditions, the percentage decrease of the $2f$ torque ripple gained from the disturbance injection is on average more than 80% of the ripple before the use of correction algorithm. It has been demonstrated that the disturbance injection to obtain better performances has to adapt to the condition of the machine controlled with fixed load speed and changing torque demand, while it is almost constant considering the case with fixed torque and changing speed. The percentage decrease of the 100 Hz torque ripple changes with disturbance injection and therefore for the first case it is not constant while for the second case it is, as it can be seen from the figures in the previous chapter.

There has not been enough time to finish to analyse the behaviour of the system in relation to the angle phase of the disturbance injection, it could be a good point to study in deep because it is not described on papers and it could help to close the loop.

At the end of this master thesis job, some future developments are proposed.

1. First of all is necessary to complete the analysis on the phase angle of disturbance injection. As described in section 5.4, a comparison between the angle corresponding to 100 Hz of FFT analysis of impedance Z from simulations with optimal injection and the behaviour of the equivalent model of the machine supplied by the fundamental voltage and a voltage waveform similar to disturbance injection could be very helpful.

2. Once found the correlation between working point and optimal injection (both amplitude and phase angle), it is possible to find out a way to adapt one of the proposed methods from the papers to the studied model. A closed-loop algorithm should work in a better way than the open-loop case.

3. Comparison of results using feedback modulation scheme, frequency modulation scheme and the presence or not of the *2f* filter at the *DC* side of the system.

4. At the end, when the simulations show the possible improvements and the control system is working properly in different conditions and with different control strategies, experimental tests can be done to check.

A

APPENDIX

This appendix is presenting the shape of output inverter currents and the machine's behaviour comparison between two-level inverter from [16] and three-level inverter used in this master job.

A.1 TWO-LEVEL MODULATION STRATEGIES

To limit the harmonic content in the output waveforms of voltages and currents in the load connected to the inverter, different modulation strategies are chosen for the two-level inverter:

1. Space Vector Modulation (SVM);
2. Selective Harmonic Elimination (SHE) with one switching angle;
3. Selective Harmonic Elimination (SHE) with two switching angles.

SVM is widely used in industrial applications because it is easy to realize and control through a digital device. In this technique, the voltage vector reference can be written as the sum of two adjacent active voltage vectors and zero vector. Once the reference voltage is known, it is easy to detect which vectors can reproduce it using a weighted sum. This process is repeated every sample time and it uses a specific algorithm.

The specific case studied in [16] uses an equivalent sine-triangular PWM technique based on SVM instead of the classic one to avoid the complexity of implementation of the conventional strategy. In this case, three-phase reference voltages are compared with the triangular carrier as in the sine-PWM; unlike the traditional technique, the sine voltage references are modified in order to obtain the same peak as in the SVM adding the common mode voltage.

SHE is a technique through which removing low-order harmonics from a given voltage is possible. Voltage references are chosen with half-wave and quarter- wave symmetry, therefore their Fourier series spectrum has only odd harmonics and can be expressed as in the equation (A.1).

$$V_{AO} = \sum_{n=odd}^{\infty} \frac{4V_{DC}}{n\pi}(1 - 2\cos n\alpha)\sin(n\omega t) \tag{A.1}$$

where α is the switching angle.

Referring to the fundamental pole voltage ($V_{AO} = \frac{4V_{DC}}{\pi}(1-2\cos\alpha)\sin(\omega t)$), the wave form amplitude can change from $4V_{DC}/\pi$ to 0 varying the

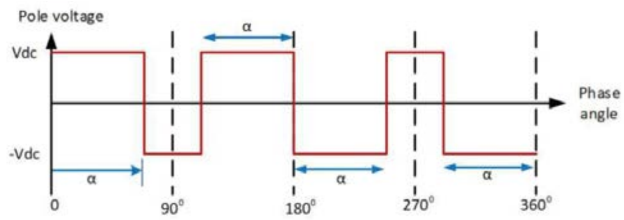

(a) *One switching angle*

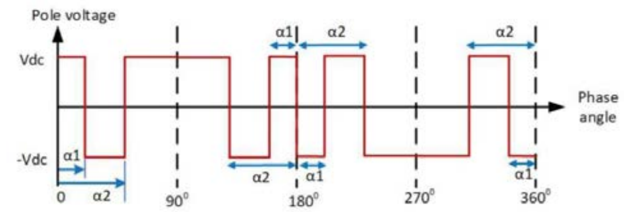

(b) *Two switching angles*

Figure A.1: Selective harmonic elimination basic idea

switching angle α from $\pi/3$ rad to $\pi/2$. Thus, the amplitude of the fundamental voltage can be varied by changing the switching angle.

Using SHE with two switching angles, the amplitude of the fundamental voltage can be varied and a specific harmonic amplitude can be eliminated. Practically, the number of switching angles corresponds to the degrees of freedom.

In this case, the Fourier series spectrum can be expressed as the equation (A.2), numerical methods are used to solve these non-linear equations and find out α_1 and α_2, which will be used during the implementation through look-up tables.

$$V_{AO} = \sum_{n=odd}^{\infty} \frac{4V_{DC}}{n\pi}(1 - 2\cos n\alpha_1 + 2\cos n\alpha_2)\sin(n\omega t) \tag{A.2}$$

The basic idea of switching angles is illustrated in fig. A.1.

A.2 2L INVERTER AND 3L INVERTER COMPARISON RESULT

In this part, graphic results are compared. As said in the previous section, the two-level inverter is controlled using three different techniques, while three-level using sinusoidal PWM with triple harmonic injection because other techniques are difficult to implement.

DC bus voltages for different inverters with their different modulation techniques are reported in figures A.2, A.3, A.4 and A.5.
Output inverter phase currents and phase to phase voltages for the four differrent cases are reported in A.6, A.7, A.8 and A.9.
In the end, torque and rotor speed for the different configurations are reported in figure A.10, figure A.11, figure A.12 and figure A.13.

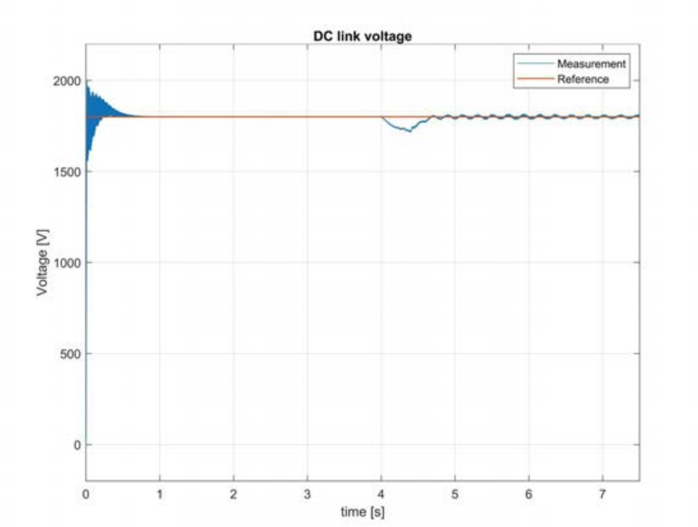

Figure A.2: DC bus voltage - two level inverter SVM

	SVM	SHE-1	SHE-2	3L
Peak-to-peak [V]	27.41	46.92	130.62	27.97
THD [%]	2.96	3.02	3.16	2.96
ripple [%]	0.056	0.054	0.056	0.056

Table A.1: DC-bus voltage comparison

The behaviours of *DC* voltage with different conditions are similar, the Total Harmonic Distortion (THD) content is low for each case, the main difference is for the peak to peak value as it can be seen in table A.1. SHE modulations present higher oscillations from the reference compared to SVM for two-level inverter and PWM for 3L-NPC inverter.

The most obvious differences are evident in currents and torque. As reported in table A.2 and A.3, the THD content, the amplitude and the percentage ripple are much better in the model where the three-level inverter is used. This is possible because with this kind of inverter, the sinusoidal reference is easier to follow because the output phase to phase voltage can assume two more levels than two-level inverter, this is evident in fig. A.9.

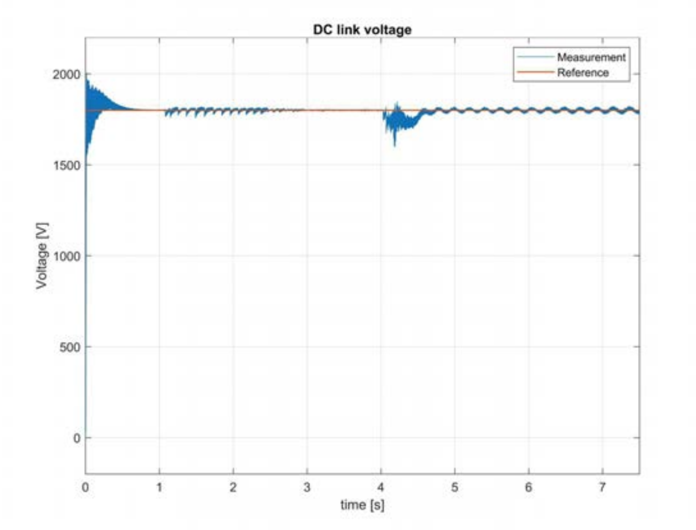

Figure A.3: DC bus voltage - two level inverter SHE one angle

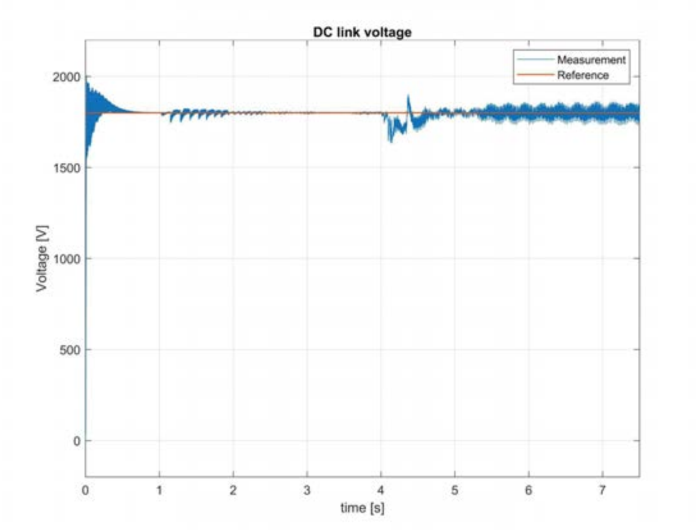

Figure A.4: DC bus voltage - two level inverter SHE two angles

	SVM	SHE-1	SHE-2	3L
Peak-to-peak [Nm]	777.2	1896.0	3067.7	511.6
THD [%]	7.47	45.8	46.33	7.17
ripple [%]	0.12	2.36	1.21	0.018

Table A.2: Torque comparison

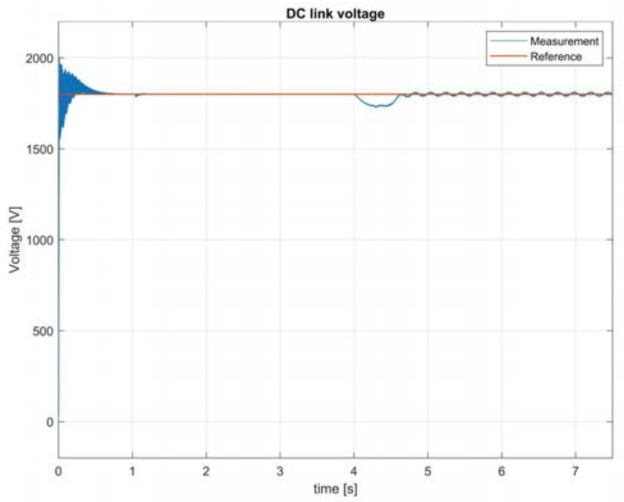

Figure A.5: DC bus voltage - three level inverter

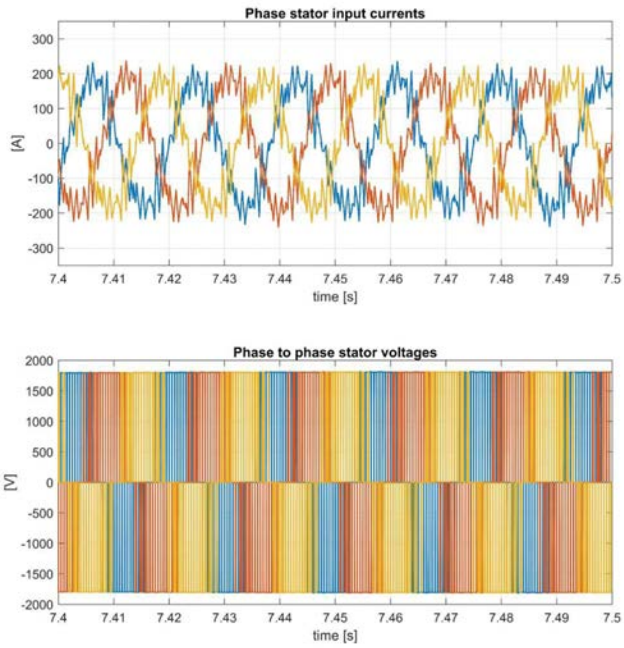

Figure A.6: Phase current and phase to phase voltage - two level inverter SVM

	SVM	SHE-1	SHE-2	3L
THD [%]	23.79	53.47	71.42	13.38

Table A.3: Current comparison

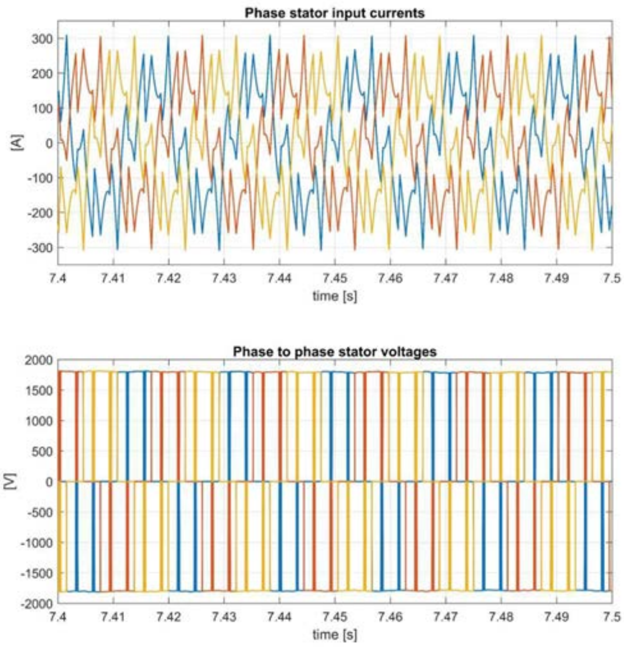

Figure A.7: Phase current and phase to phase voltage - two level inverter SHE one angle

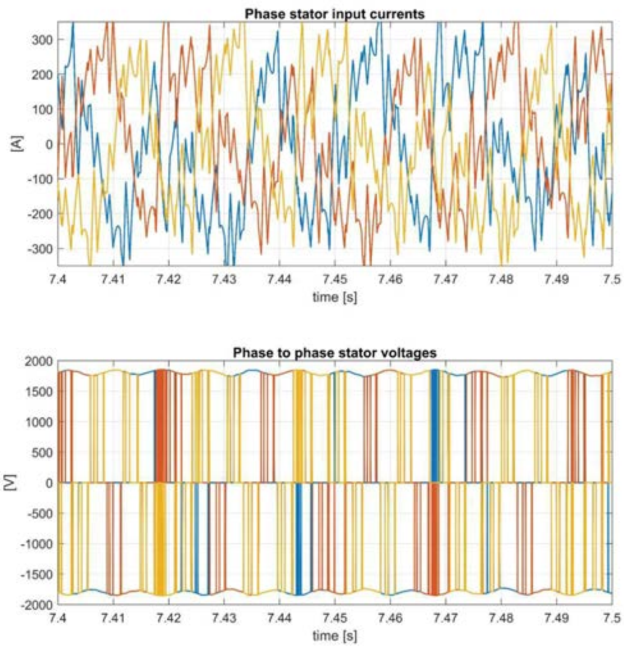

Figure A.8: Phase current and phase to phase voltage - two level inverter SHE two angles

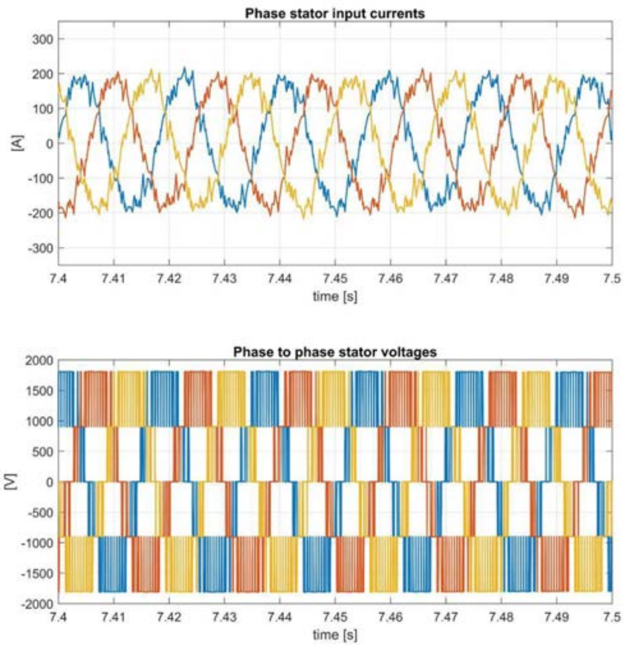

Figure A.9: Phase current and phase to phase voltage - three level inverter

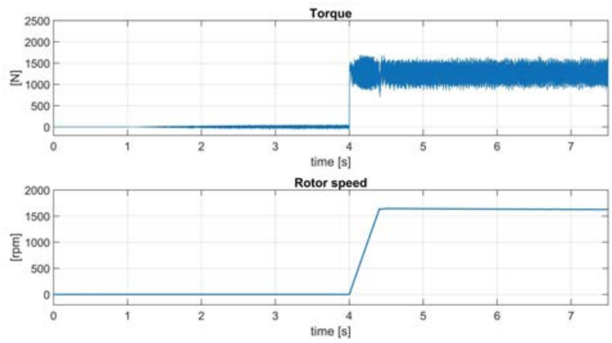

Figure A.10: Torque and speed - two level inverter SVM

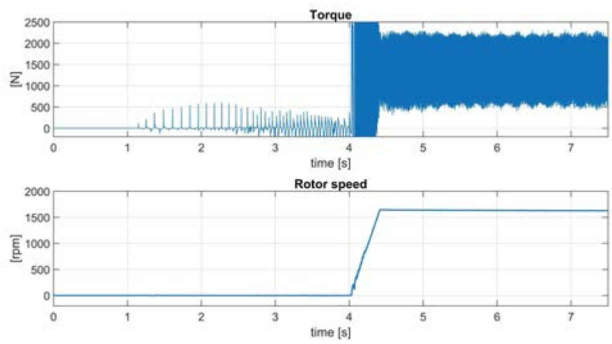

Figure A.11: Torque and speed - two level inverter SHE one angle

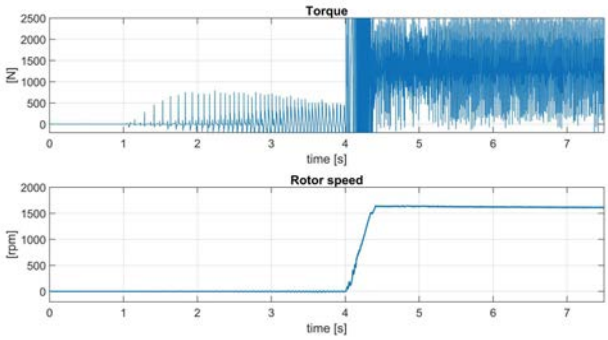

Figure A.12: Torque and speed - two level inverter SHE two angles

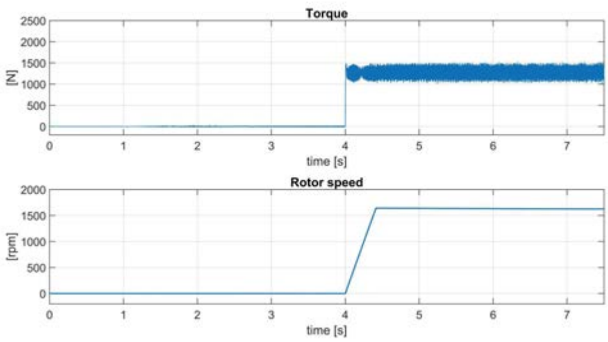

Figure A.13: Torque and speed - three level inverter

BIBLIOGRAPHY

[1] Fernando Briz. "Control of induction machines." In: *Dynamic Control of AC machines (Class slides)*. 2019.

[2] M. Ciobotaru, R. Teodorescu, and F. Blaabjerg. "A new single-phase PLL structure based on second order generalized integrator." In: *2006 37th IEEE Power Electronics Specialists Conference*. 2006, pp. 1–6.

[3] Ratna BABU Deekollu. "Vector Control of Three Phase Active Rectifier with Lower Input Current Harmonic Distortion and Unity Power factor using Space Vector Modulation." In: *ResearchGate* (2016).

[4] Prasad N Enjeti and Wajiha Shireen. "A new technique to reject DC-link voltage ripple for inverters operating on programmed PWM waveforms." In: *IEEE Transactions on Power Electronics* 7.1 (1992), pp. 171–180.

[5] Eurostat. *Energy, transport and enviromental statistics - 2019 edition*. Ed. by Statistical books. European Commision, 2019.

[6] Xinglai Ge, Xiaoyun Feng, Baisi Liu, and Shihao Chen. "Beat-less control technology and its application in three-level inverter." In: *2008 International Conference on Electrical Machines and Systems*. IEEE. 2008, pp. 1763–1767.

[7] Bin Gou, Xiaoyun Feng, Wensheng Song, Kun Han, and Xinglai Ge. "Analysis and compensation of beat phenomenon for railway traction drive system fed with fluctuating DC-link voltage." In: *Proceedings of The 7th International Power Electronics and Motion Control Conference*. Vol. 1. IEEE. 2012, pp. 654–659.

[8] Michal Hrkel, Ján Vittek, and Zdeno Biel. "Maximum torque per ampere control strategy of induction motor with iron losses." In: *2012 ELEKTRO*. IEEE. 2012, pp. 185–190.

[9] Yanxiao Lei, Ke Wang, Lu Zhao, and Qiongxuan Ge. "An improved beatless control method of AC drives for railway traction converters." In: *2016 19th International Conference on Electrical Machines and Systems (ICEMS)*. IEEE. 2016, pp. 1–5.

[10] Miroslav Macan, Ivan Bahun, and Željko Jakopović. "Output dc voltage elimination in pwm converters for railway applications." In: *International Conference on Electrical Drives and Power Electronics (17; 2011)*. 2011.

[11] Rushikesh Mali, Nitin Adam, Akshay Satpaise, and AP Vaidya. "Performance Comparison of Two Level Inverter with Classical Multilevel Inverter Topologies." In: *2019 IEEE International Conference on Electrical, Computer and Communication Technologies (ICECCT)*. IEEE. 2019, pp. 1–7.

[12] Ned Mohan, Tore M Undeland, and William P Robbins. *Power electronics: converters, applications, and design*. John wiley & sons, 2003.

[13] Kiyoshi Nakata, Tokunosuke Nakamachi, and Kiyoshi Nakamura. "A beatless control of inverter-induction motor system driven by a rippled dc power source." In: *Electrical engineering in Japan* 109.5 (1989), pp. 122–131.

[14] Milton E de Oliveira Filho, Jonas R Gazoli, Alfeu J Sguarezi Filho, and Ernesto Ruppert Filho. "A control method for voltage source inverter without dc link capacitor." In: *2008 IEEE Power Electronics Specialists Conference*. IEEE. 2008, pp. 4432–4437.

[15] Ahmed Omar, Mona Fouad, Adel El-rfaey, and Yasser Gaber. "DC offset compensation technique for grid connected inverters." In: *2018 9th International Renewable Energy Congress (IREC)*. IEEE. 2018, pp. 1–7.

[16] Pahan Chamika Oruthota. "Efficient Control and Modulation Strategies for High Speed AC Drives for Electric Traction." MA thesis. Universidad de Oviedo, 2019.

[17] Mario Schweizer, Thomas Friedli, and Johann W Kolar. "Comparative evaluation of advanced three-phase three-level inverter/converter topologies against two-level systems." In: *IEEE Transactions on industrial electronics* 60.12 (2012), pp. 5515–5527.

[18] Andreas Steimel. *Electric traction-motive power and energy supply: basics and practical experience*. Oldenbourg Industrieverlag, 2008.

[19] Roberto Turri. "Trazione elettrica." In: *Sistemi elettrici per l'industria e i trasporti (Class Slides and Reports)*. A.A. 2018/2019.

[20] Hani Vahedi and Kamal Al-Haddad. "Half-bridge based multilevel inverter generating higher voltage and power." In: *2013 IEEE Electrical Power & Energy Conference*. IEEE. 2013, pp. 1–6.

[21] Laura Guerrero Viejo. "2F Filter Elimination for Railway Applications." MA thesis. Universidad de Oviedo, July 2018.

[22] Gaolin Wang, Chaohui Yu, Nannan Zhao, and Dianguo Xu. "Beat-less control of electrolytic capacitor-less air conditioning motor drive system." In: *2017 IEEE Transportation Electrification Conference and Expo, Asia-Pacific (ITEC Asia-Pacific)*. IEEE. 2017, pp. 1–5.

[23] Yaosuo Xue and Liuchen Chang. "Closed-loop SPWM control for grid-connected buck-boost inverters." In: *2004 IEEE 35th Annual Power Electronics Specialists Conference (IEEE Cat. No. 04CH37551)*. Vol. 5. IEEE. 2004, pp. 3366–3371.